

Evolution and final fates of low- and intermediate-mass stars

Alessandro Bressan^a and Kendall Gale Shepherd^a

^aSISSA, Physics Department, Via Bonomea 265, Trieste Italy

© 20xx Elsevier Ltd. All rights reserved.

Chapter Article tagline: update of previous edition., reprint..

Abstract

Stars are unique bodies of the Universe where self-gravity compress matter to such high temperature and density that several nuclear fusion reactions ignite, providing enough feedback against further compression for a time that can be even larger than the age of the universe. The main property of a star is its mass because it determines its structure, evolutionary history, age, and ultimate fate. Depending on this quantity, stars are broadly classified as low-mass stars, like our Sun, intermediate mass stars as the variable star Delta Cephei, and massive stars as Betelgeuse, a red supergiant star in Orion constellation. Here we will introduce the basic notions useful to understand stellar evolution of low- and intermediate- mass stars. This mass range ($0.1 M_{\odot} - 10.0 M_{\odot}$) deserves special attention, as it contains most of the stars in the universe. This chapter will focus on how these stars form, the processes that drive their evolution, and key details regarding their structure. Finally, we will discuss the death of such stars, emphasizing the unique fates associated with low- and intermediate-mass stars.

Glossary

Nomenclature

AGB	Asymptotic Giant Branch - section 9.1
CMD	The Colour Magnitude Diagram - section 3.8
EOS	The equation of state of stellar plasma - section 3.1
HB	Horizontal Branch - section 7
HRD	The Hertzsprung-Russell Diagram - section 3.8
MLT	Mixing Length Theory of convection - section 3.3.2
MS	Main Sequence - section 5
PAGB	Post Asymptotic Giant Branch - section 9.2
RGB	Red Giant Branch - section 6
SAGB	Super-Asymptotic Giant Branch - section 9.1
SGB	Sub Giant Branch - section 6.1
TRGB	The tip of the RGB - section 6.3
WD	White Dwarf - section 10
ZAMS	Zero Age Main Sequence - section 5

1 Objectives

- The system of equations of the stellar structure
- Chemical composition of stars
- The Hertzsprung-Russell Diagram
- Hydrogen burning- and Helium burning- nuclear reactions
- Main sequence stars
- Stellar lifetimes
- Sub giant stars
- Electron degeneracy
- Red Giant stars
- Horizontal Branch stars
- Asymptotic Giant Branch stars
- White Dwarfs

2 Introduction

In this chapter we will describe the evolution of low- and intermediate- mass stars, namely stars whose initial mass is from one tenth to about ten times that of the Sun. Section 3 will deal with the basic but general equations that govern the stellar structure, essentially the mass, momentum and energy conservation, and the equation of energy transport. The method of solution will also be briefly discussed, and a list of existing numerical codes adopted by different authors will be provided. In the following sections we will describe the evolution of low-mass stars during the Pre-Main Sequence phase (section 4) that is, just after their formation; the Main Sequence phase (section 5), where stars burn their central Hydrogen (H); the Red Giant phase with the Helium (He) Flash at He ignition (section 6); the Horizontal Branch (section 7) where low mass stars burn their central He. Section 8 will briefly review the evolution of intermediate mass stars until central He exhaustion while, the final nuclear phases of low- and intermediate-mass stars, being very similar, will be discussed together in section 9. In section 10, we will discuss how the final fate of such stars is approached, without knowing if an end really exists. This chapter is meant to provide a broad overview on low- and intermediate-mass stars, and therefore some topics are treated concisely for the sake of brevity. We refer the reader to specific textbooks cited in the text for more details.

3 The structure of stars

While discussing stellar structure and evolution it is unavoidable to refer to the Sun. A few preliminary considerations concerning the Sun are useful to introduce the reader to the realm of stars. The Sun is the star nearest to us; the Earth orbits around the Sun at an average distance of 150 million km in a period of time called a year, which corresponds to 3.1×10^7 seconds, or about 365.25 days. Nevertheless the Sun's luminosity is so high that the heat captured by the Earth helps life to develop and evolve on its surface. Its age is estimated to be about 4.5 billion years. Its distance from the other nearest star, Proxima Centauri, is about 4.23 light-years¹. Therefore, the Sun is an isolated star, and its structure and evolution depend only on its intrinsic properties².

Evidence suggests that the geometry of the Sun can be very well approximated by a sphere. All other stars are so distant that we see them as point-like sources³. Besides the evidence, spherical symmetry is also prompted by self-gravity and it is usually a good approximation. In a spherically symmetric model all physical quantities depend only on the radial coordinate, so that a three dimensional real star can be described with an one dimensional model. The benefits of using a one dimensional model will become apparent in the following sections. However deviations from spherical symmetry may arise because of non-central forces, like those originating from rotation and magnetic fields. These effects will not be considered here (but see e.g. Maeder, 2009; Low, 2001).

We will now derive the equations that regulate the stellar structure assuming a spherical configuration. We first define the following basic quantities at a given radial distance from the center, r . The mass enclosed within the sphere of radius r is $m(r)$, $\rho(r)$ the matter density, $P(r)$ the pressure, $T(r)$ the temperature, $L(r)$ the local luminosity (the energy flowing through the surface of radius r per unit time), $\epsilon_{\text{nuc}}(r)$ is the energy generated by nuclear reactions per unit mass and time, $\epsilon_{\nu}(r)$ is the energy lost in form of neutrinos per unit mass and time, $s(r)$ is the specific entropy (i.e. the entropy per unit mass). All of the above quantities are constant on the surface of a sphere of radius r , and the problem of defining the structure of a star is that of describing their variation over a radial displacement between r and a nearby location $r + dr$ (differential equations), plus that of finding their initial values, the so called initial conditions.

3.1 The mass conservation

In the case of the mass enclosed by the spherical surface at r , $m(r)$, its variation is simply the mass contained by the spherical shell limited by r and $r + dr$, whose volume is $dV = 4\pi r^2 dr$. Thus the first differential equation of the stellar structure, stating the principle of mass conservation, writes (Kippenhahn et al., 2013; Maeder, 2009)

$$\frac{\partial m}{\partial r} = 4\pi r^2 \rho. \quad (1)$$

This differential equation involves two dependent functions of the independent variable r , $m(r)$ and $\rho(r)$ and at least another differential equation involving the same functions must be found to get a viable solution. We note that the matter density $\rho(r)$ is related to the pressure $P(r)$ and the temperature $T(r)$ through the equation of state (EOS).

3.2 The hydrostatic equilibrium

A differential equation for the internal pressure can be obtained by considering that the Sun has maintained its size almost unchanged for at least centuries. This indicates that the attraction by gravity at any point in its interior is balanced by another force, otherwise the Sun would collapse in a dynamical timescale, which is less than a fraction of a hour. We say that the Sun satisfies the conditions for the hydrostatic equilibrium, with the balancing force being provided by the pressure gradient, $\partial P/\partial r$. Equating the outward acceleration due to the radial

¹A light-year (ly) corresponds to 9.461×10^{17} cm; 1 parsec is 3.26156 ly.

²Notable exceptions are tight binaries or other multiple stellar systems where individual components feel the effects of the nearby companions.

³Only a few other stars are sufficiently near to us that we may obtain an extended image, i.e. a non point-like image.

pressure gradient and the inward acceleration due to gravity we get

$$-\frac{1}{\rho} \frac{\partial P}{\partial r} - \frac{Gm}{r^2} = 0. \quad (2)$$

Note that the quantity $\partial P/\partial r$ is negative so that the first term in the left hand side of Equation (2) is positive and directed outward while the acceleration of gravity is negative and directed inward (opposite of the radial vector).

Hydrostatic Equilibrium

Central pressure and central temperature

Equation (1) and Equation (2) can be combined to give (see e.g. [Kippenhahn et al., 2013](#))

$$\frac{\partial P}{\partial m} = -\frac{Gm}{4\pi r^4}. \quad (3)$$

From Equation (3) we can get an order of magnitude estimate for central pressure

$$\begin{aligned} \frac{P_{\text{central}} - P_{\text{surface}}}{m_{\text{central}} - m_{\text{surface}}} &\approx -\frac{GM}{4\pi R^4} \\ P_{\text{central}} &\approx \frac{GM^2}{4\pi R^4} \approx \frac{6.67 \cdot 10^{-8} (2 \times 10^{33})^2}{4\pi (7 \times 10^{10})^4} \text{ dyn cm}^{-2} \approx 10^{15} \text{ dyn cm}^{-2}, \end{aligned} \quad (4)$$

where we have assumed for the Sun $M_{\odot} \sim 2 \times 10^{33}$ g and $R_{\odot} \sim 7 \times 10^{10}$ cm together with $M_{\text{central}}=0$ and $P_{\text{surface}}=0$.

If M and V are the mass and the volume of the gas, and \mathcal{N} the number of atoms such that, e.g. for pure H, $M = \mathcal{N}m_{\text{H}}$, the perfect gas law equation of state is $P V = \mathcal{N} k_{\text{B}} T$. Since $\mathcal{N} = M/m_{\text{H}}$ and noting that $\rho = M/V$ we can write

$$P = \frac{\rho}{m_{\text{H}}} k_{\text{B}} T. \quad (5)$$

Then, using for the density ρ its average value in the Sun $M_{\odot}/(\frac{4}{3} \pi R_{\odot}^3) \approx 1 \text{ g cm}^{-3}$ we get an order of magnitude estimate of the central temperature

$$T_{\text{central}} \approx 10^{15} \frac{m_{\text{H}}}{\rho k_{\text{B}}} \approx 1.2 \times 10^7 \text{ K}. \quad (6)$$

The dynamical timescale.

In case the condition for the hydrostatic equilibrium is violated, an interior mass element is subject to a residual acceleration

$$\frac{\partial^2 r}{\partial t^2} = -\frac{1}{\rho} \frac{\partial P}{\partial r} - \frac{Gm}{r^2}. \quad (7)$$

Assuming that the unbalance between gravity and pressure gradient is a fraction f of the gravity, then

$$\frac{\partial^2 r}{\partial t^2} = f \frac{Gm}{r^2}, \quad (8)$$

and the corresponding dynamical timescale would be

$$t_{\text{d}}^2 = \frac{1}{fG \frac{m}{r^3}} \approx \frac{1}{4fG < \rho(r) >}. \quad (9)$$

Again, using the average density of the Sun and assuming $f \sim 1$, $t_{\text{d}} \sim 30$ min, meaning that if the Sun were not in hydrostatic equilibrium, it should appreciably change its radius in a timescale of about 30 min (e.g. [Kippenhahn et al., 2013](#)). Conversely, the slowness with which the Sun is actually changing its radius suggests that it follows the hydrostatic equilibrium to an extremely great precision. Indeed, accurate time domain observations from helioseismology indicate that the Sun oscillates at frequencies that are in agreement with Equation (9) ([Buldgen et al., 2019](#), and references therein).

3.3 The temperature gradient

In general, Equation (1) and Equation (2) are not enough to close the system of differential equations of the stellar structure because they involve three dependent functions of the independent variable r^4 . Using the equation of state will generally introduce another dependent function of radius, the temperature T , and a new differential equation for $T(r)$ must be introduced. The equation for the change of the temperature with radius is strictly connected with the mechanism responsible for the energy transport within stars.

From laboratory experiments we know that there are at least three main processes to transport energy within a medium. One is conduction by free electrons, the other is convection by moving fluid elements, and the third one is radiation by photons. Within stars the main mechanisms are radiation and convection, while conduction becomes important only in particular conditions.

⁴A favorable condition arises when the pressure is a function of only the density. In that case the structure can be defined by the two equations (1) and (2) if suitable boundary conditions are found, because they involve only two dependent functions of radius, the pressure $P(r)$ and the mass $m(r)$.

4 Evolution and final fates of low- and intermediate-mass stars

The mean free path of photons in the interiors of our Sun is of the order of a few centimeters

The mean free path refers to the average distance travelled by a particle in between collisions. For photons, we get it by multiplying the average time between collisions (τ_{coll}) of photons with electrons, by the velocity of the photons. τ_{coll} is the reciprocal of the number of collisions per unit time, N_{coll} . N_{coll} is the number of possible collisions with electrons within the effective volume swept up by a moving cross-section of the photon-electron interaction, per unit time. For example, for the Thomson scattering of photons by free electrons in an ionized plasma, N_{coll} is the product of the number density of electrons (n_e) times the volume of the cylinder with base σ_T and height $h = v_{\text{phot}} \tau_{\text{coll}}$: $N_{\text{coll}} = n_e \sigma_T v_{\text{phot}} \tau_{\text{coll}}$. Thus the mean free path ℓ_{phot} is

$$\ell_{\text{phot}} = v_{\text{phot}} \tau_{\text{coll}} = \frac{v_{\text{phot}}}{N_{\text{coll}}} = \frac{v_{\text{phot}}}{n_e \sigma_T v_{\text{phot}}} = \frac{1}{n_e \sigma_T} . \quad (10)$$

The mean free path of a particle for a certain interaction does not depend on the relative velocity of the colliding particles. The cross section of the Thomson scattering is $\sigma_T \approx 6.6525 \cdot 10^{-25} \text{ cm}^2$ and $n_e \approx \rho/m_H \text{ cm}^{-3}$. For the interior of the Sun, $\rho \geq 1 \text{ g cm}^{-3}$ and with $m_H = 1.6735 \times 10^{-24} \text{ g}$ we get

$$\ell_{\text{phot}} = \frac{1}{n_e \sigma_T} = \frac{m_H}{\rho \sigma_T} \leq \frac{1.67 \times 10^{-24}}{1. \times 6.65 \times 10^{-25}} \approx 2.5 \text{ cm} . \quad (11)$$

Thus, photons within the Sun travel, on average, a few centimeters or even less between each interaction.

The stellar radius and the effective temperature

Making use of the results of the theory of stellar atmospheres (e.g. [Mihalas, 1970](#)) the stellar radius is conventionally defined as the radial coordinate where the optical depth of photons against interaction with the stellar plasma, beginning from zero at infinity, reaches $2/3$ as the stellar interiors are approached: $\tau_{\text{phot}} = - \int_{\infty}^R \kappa_R \rho dr = 2/3$. The star extends beyond that radius and formally up to infinity, but with a density that becomes so low that it has no significant impact on the star. Within this external region of the star, where the photons can freely escape because $\ell_{\text{phot}}/R \gg 1$, the medium is said to be optically thin. In deeper regions τ increases and the region is said to be optically thick, being $\ell_{\text{phot}}/R \ll 1$. The thermal stellar radiation that hits our detectors thus carries information only from this narrow region where $\tau \sim 2/3$, called the photosphere.

With the luminosity and the radius, an effective temperature, T_{eff} , is defined by assuming that the emissivity at the photosphere equals that of a black body. By applying the Stefan–Boltzmann law, one gets

$$\frac{L}{4\pi R^2} = \sigma_{\text{SB}} T_{\text{eff}}^4 , \quad (12)$$

where $\sigma_{\text{SB}} = 6.670374419 \times 10^{-5} \text{ erg/s/cm}^2/\text{K}^4$ is the Stefan-Boltzmann constant. The effective temperature can be measured in several different ways (see e.g. [Smalley, 2005](#); [Gray and Kaur, 2019](#)). The nominal value for the Sun is $T_{\text{eff}\odot} = 5772 \text{ K}$ ([Prša et al., 2016](#)).

The energy transport mechanisms are responsible of keeping different stellar layers in thermal contact and they involve the knowledge of the mean free path, ℓ , of the carriers of energy, i.e. the average distance the carriers travel from the site where they absorb heat to the site where they deposit heat. This average distance depends on the particular ability of the carrier to interact with the surrounding medium, the cross section $\sigma_{\text{interaction}}$ of the interaction. In the case of conduction, a free electron acquires energy in the collision with another charged particle and travels a certain distance before the following interaction, where an exchange of energy may occur. The same is true for photons that are emitted in a hotter region and then, after traveling a certain distance, are absorbed by particles in a cooler region. Convection develops in a medium within a gravity field when hotter (and less dense) macroscopic bubbles move because of the Archimedes buoyant force. In that case the mean free path of the bubbles is called the mixing length, because it is supposed that bubbles keep their identity until they mix with the surrounding medium (e.g. [Böhm-Vitense, 1958](#)). Generally, the larger the mean free path of a carrier, the more efficient it is in transporting energy. For photons and electrons, the mean free path is calculated by considering the average distance traveled between two subsequent collisions.

Adjacent layers of matter within the Sun are in thermal equilibrium

Adjacent means that the layers are at a distance of a photon mean free path so that radiation may keep them in thermal contact. For the central temperature of the Sun, the estimate derived from the hydrostatic equilibrium equation gives $T_{\text{central}} \approx 10^7 \text{ K}$. The average temperature gradient within the Sun, dT/dr , is then

$$\frac{T_{\text{central}} - T_{\text{surface}}}{R_{\text{central}} - R_{\text{surface}}} \sim - \frac{T_{\text{central}}}{R_{\text{surface}}} = - \frac{10^7}{7 \times 10^{10}} \approx - 1.4 \times 10^{-4} \text{ K cm}^{-1} . \quad (13)$$

The temperature variation over a photon mean free path is $\delta T \approx dT/dr \times \ell \approx 1.4 \times 10^{-4} \times 2.5 = 3.5 \times 10^{-4} \text{ K}$. What matters is the relative temperature variation, which is $\delta T/T \approx 3.5 \times 10^{-4}/10^7$. So, the relative temperature variation between shells of matter kept in contact by photons is $\delta T/T \approx 3.5 \times 10^{-11}$. Thus, internal layers are “locally” in thermal equilibrium (their relative temperature difference is negligibly small). Since the layers are also in hydrostatic equilibrium, we say that they are in Local Thermodynamic Equilibrium (LTE). The star, as a whole, is not in thermodynamic equilibrium because it is an open system that is losing energy through photons, neutrinos and even mass flows.

3.3.1 Radiative energy transport

The relative short length of the photon mean free path, Equation (11), with respect to the radius of the Sun suggests that the energy transport by photons is a diffusive process. In this case the density of the energy flux, $L/4\pi r^2$, is proportional to the gradient of the energy density of

radiation, $U = aT^4$, where $a = 4\sigma_{\text{SB}}/c$, is the radiation constant. The constant of proportionality is the diffusion coefficient which has the form

$$D = \frac{1}{3}c\ell, \quad (14)$$

where c is the speed of light and ℓ is the photon mean free path. The density of the energy flux for the radiative transport is thus

$$\frac{L}{4\pi r^2} = -\frac{1}{3}c\frac{1}{n_e\sigma_T}\nabla U = -\frac{4ac}{3}\frac{T^3}{n_e\sigma_T}\frac{dT}{dr}.$$

Inverting this equation, we get the temperature gradient equation for the radiative transport

$$\frac{dT}{dr} = -\frac{3n_e\sigma_T}{4acT^3}\frac{L}{4\pi r^2}. \quad (15)$$

In Equation (15) we made use of the microscopic Thomson cross section for the scattering of photons by free non relativistic electrons. With more generality we may consider other processes, including interactions of photons with atomic bound electrons (bound-bound interactions), photo-ionization (bound-free interactions), interactions with free electrons near charged particles (free-free), Compton (for energetic photons) scattering and also interactions with molecules. These interactions depend on the frequency of the photons and to include them into Equation (15), one must consider a suitable average over the whole frequency range of radiation. It has been shown that a suitable mean free path for photons can be obtained using the Rosseland mean opacity of stellar matter κ_{R} [cm^2g^{-1}] (Rosseland, 1924)

$$\ell = \frac{1}{\kappa_{\text{R}} \times \rho}, \quad (16)$$

where κ_{R} is a function of temperature, density and elemental abundance of a specific stellar layer, i.e. $\kappa_{\text{R}} = \kappa_{\text{R}}[T(r), \rho(r), X_i(r)]$. Here and later, the term X_i indicates the abundance by mass fraction of all the elements that are explicitly considered in the calculation of a stellar structure.

Using the Rosseland mean opacity, which is computed in several laboratories, the temperature gradient equation for the radiative transport can be written as (e.g. Weiss et al., 2004)⁵

$$\frac{\partial T}{\partial r} = \frac{\partial T}{\partial r}\Big|_{\text{Rad}} = -\frac{3\kappa_{\text{R}}\rho}{4acT^3}\frac{L}{4\pi r^2}. \quad (17)$$

3.3.2 Convective energy transport

Equation (17) states that energy that diffuses outward by radiation establishes a local negative temperature gradient whose absolute value increases with increasing opacity (κ_{R}) or with increasing flux density ($L/4\pi r^2$). Laboratory experiments on convection show that, if the absolute value of the local temperature gradient exceeds the adiabatic one, the medium become unstable and convection sets in, becoming the most efficient energy transport mechanism. Making use of the logarithmic temperature versus pressure gradient $\nabla = (d\ln T / d\ln P) = (P/T)(dT/dP)$, the condition to adopt either the radiative or the adiabatic gradient in Equation (17) is (see e.g. Kippenhahn et al., 2013)⁶:

$$\begin{aligned} \nabla &= \nabla_{\text{Rad}} & \text{if } \nabla_{\text{Rad}} < \nabla_{\text{Adi}} & \text{ (stable)} \\ \nabla &= \nabla_{\text{Adi}} & \text{if } \nabla_{\text{Rad}} \geq \nabla_{\text{Adi}} & \text{ (unstable)}. \end{aligned} \quad (18)$$

In Equation (18), ∇_{Rad} and ∇_{Adi} are the values of the radiative gradient needed to transport the luminosity calculated with Equation (17), and the gradient of a quasi-static thermodynamic adiabatic process, respectively. Both ∇_{Rad} and ∇_{Adi} can be calculated from the local values of T , ρ , X_i , of the structure. Equation (18) states the Schwarzschild criterion for stability against convection (named after Karl Schwarzschild). Since a negative gradient of mean molecular weight favors stability, a more stringent condition is often used, the Ledoux one (named after Paul Ledoux)⁷.

The Sun's convective zones produce currents of plasma, that cause the appearance of granules at the top of the convective cells. The Solar granulation observed at the Sun's photosphere (Bahng and Schwarzschild, 1961), is therefore indicative of the presence of convective currents. Helioseismology shows that solar convection extends from the surface down to the 71.3% of the solar radius (Basu and Antia, 1997). Below that point, radiation is able to transport the energy flux without destabilizing the plasma. The geometric size of these convective cells offer useful indicators of the scale of this process, which cannot be determined from first physical principles.

In the more external regions of a star, convective energy transport may become inefficient due to the low density of the medium. Though very thin in mass, these regions may contribute to a significant fraction of the stellar radius (because of the low density), and so they may have a significant impact on the effective temperature of the star. In this case, convective elements do not move adiabatically and their temperature gradient must be derived by explicitly solving the equations of the Mixing Length Theory (MLT) of convection (e.g. Böhm-Vitense, 1958; Weiss et al., 2004). This theory is based on a typical scale for convective motions, the Mixing Length (ML). The ML is one

⁵Because energy transport by electron conduction can also be treated as diffusive processes, conduction is usually accounted for by calculating a "conductive opacity", κ_{C} , and applying the following correction to the Rosseland mean opacity: $1/\kappa_{\text{tot}} = 1/\kappa_{\text{R}} + 1/\kappa_{\text{C}}$ (e.g. Cassisi et al., 2021).

⁶Note that ∇ has the opposite sign of $\frac{\partial T}{\partial r}$.

⁷Both the Schwarzschild and the Ledoux criteria define the stability of the medium against convection, but there remains an ambiguity on the real size of convective regions because convection may penetrate into the surrounding stable regions, a process named *convective overshooting* (e.g. Bressan et al., 1981).

6 Evolution and final fates of low- and intermediate-mass stars

of the more important but still uncertain parameters in stellar evolution, and it is usually determined by comparison of suitable solar models with the real Sun.

3.4 The energy conservation

The differential Equation (17) provides the variation of the temperature within the star, but the whole system of equations cannot be integrated because Equation (17) introduces the function $L(r)$, the luminosity, which is still unknown. The last term in the RHS of Equation (17) describes the amount of energy that flows per unit time and per unit area across the spherical surface at r . If there are no sources or sinks of energy, the total $L(r)$ over the whole surface, $4\pi r^2$, will be constant. Conversely, if sources and sinks are present in the mass shell $dm = 4\pi r^2 \rho dr$, and we quantify them as ϵ [$\text{erg s}^{-1} \text{g}^{-1}$], the luminosity will change by $\epsilon \times dm$, so that we may write the energy conservation as

$$\frac{\partial L}{\partial r} = 4\pi r^2 \rho \epsilon. \quad (19)$$

The main sources or sinks of energy within stars are due to nuclear reactions, work done by gravity or by pressure against gravity (contraction or expansion of stellar layers) and processes that involve neutrino production that, because of their negligible cross section with matter, escape directly from the star instead of diffusing outside like photons⁸. These terms are explicitly indicated as

$$\epsilon(r) = \epsilon_{\text{nuc}}(r) - T(r) \frac{\partial s(r, t)}{\partial t} - \epsilon_{\nu}(r), \quad (20)$$

where $\epsilon_{\text{nuc}}(T, \rho, X_i)$, $s(T, \rho, X_i)$ and $\epsilon_{\nu}(T, \rho, X_i)$, are the specific nuclear energy generation rate⁹, specific entropy and specific neutrino energy production rate (or neutrino luminosity) and are all function of temperature, density, elemental abundance X_i at a given position within the star, and where specific means that the quantities are evaluated per unit mass, so that they are all expressed in units of [$\text{erg g}^{-1} \text{s}^{-1}$]¹⁰.

3.5 The chemical abundances

The mean molecular weight

The number of particles per unit volume, $N = \mathcal{N}/V$, is often expressed by means of the mean molecular weight μ , which is the average mass per particle in AMU (e.g. [Kippenhahn et al., 2013](#)). We may derive the mean molecular weight of a mixture of elements by considering that

$$N = \frac{\rho}{\mu \mathcal{A}} = \sum_i N_i \times n_i = \frac{\rho}{\mathcal{A}} \sum_i \frac{X_i}{A_i} \times n_i, \quad (21)$$

where N_i is given by Equation (29) and n_i denotes the number of individual particles provided by the ions i (i.e. the nucleus plus the free electrons in case of ionization). Thus,

$$\frac{1}{\mu} = \sum_i \frac{X_i}{A_i} \times n_i. \quad (22)$$

Making use of the mean molecular weight, the pressure of a perfect gas becomes

$$P = k_B \frac{\rho T}{\mu \mathcal{A}}. \quad (23)$$

For a fully ionized medium

$$\frac{1}{\mu} \simeq 2 \frac{X}{A_{\text{H}}} + 3 \frac{Y}{A_{\text{He}}} + \sum_i \frac{Z_i}{A_i} \times (\mathcal{Z}_i + 1), \quad (24)$$

where \mathcal{Z}_i and Z_i are the atomic number (charge) and the abundance by mass of the i element other than H and He, respectively. A good approximation is to set $A_{\text{H}}=1$, $A_{\text{He}}=4$ and $\mathcal{Z}_i + 1 \simeq A_i/2$ so that

$$\frac{1}{\mu} \simeq 2X + \frac{3}{4}Y + \sum_i \frac{Z_i}{A_i} \times \frac{A_i}{2} = 2X + \frac{3}{4}Y + \frac{\sum_i Z_i}{2} = 2X + \frac{3}{4}Y + \frac{Z}{2}. \quad (25)$$

If we are interested in the electron pressure and we only count electrons then, for full ionization of the same mixture, we have

$$\frac{1}{\mu_e} \simeq X + \frac{2}{4}Y + \sum_i \frac{Z_i}{A_i} \times \frac{A_i}{2} = X + \frac{1}{2}Y + \frac{\sum_i Z_i}{2} = X + \frac{Y}{2} + \frac{Z}{2} = \frac{1+X}{2}, \quad (26)$$

and, for ions

$$\frac{1}{\mu_{\text{ions}}} \simeq X + \frac{Y}{4} + \sum_i \frac{Z_i}{A_i}. \quad (27)$$

⁸An exception is the formation of a neutrino-sphere during the final collapse of massive stars (e.g. [Burrows and Vartanyan, 2021](#)).

⁹Nuclear reaction rates must account for the screening of the nuclear charge by the electron gas (e.g. [Salpeter, 1954](#)).

¹⁰Terms not included here are e.g. kinetic energy rates associated with mass loss or mass accretion rates, heating and/or tidal effects by binary companions, energy production rates by exotic dark matter interactions, etc.

In stellar astrophysics the capital letters X , Y and Z are used to indicate the fractional abundance by mass of H, He and all remaining elements, called “metals”, at a given position r within the star, respectively. Because by definition $X = X_{\text{H}} = \rho_{\text{H}}/\rho$ and similar definitions hold for He and metals,

$$X + Y + Z = \frac{\rho_{\text{H}} + \rho_{\text{He}} + \rho_{\text{M}}}{\rho} = 1. \quad (28)$$

If we follow the abundances of specific elements in detail then we need to write $\sum X_i = 1$, and now X_i refers to the i^{th} element in our list. The equation of state requires the knowledge of the number of atoms of the element i per unit volume, N_i . This can be derived by dividing the density of the element i , ρ_i , by its mass in grams

$$N_i = \frac{\rho_i}{A_i \mathcal{A}} = \rho \frac{X_i}{A_i \mathcal{A}}, \quad (29)$$

where A_i is the (atomic) mass of element i expressed in Atomic Mass Unit [AMU], \mathcal{A} ¹¹. The quantity X_i/A_i is often indicated with Y_i which, by definition, indicates the number of moles per gram of the element i .

3.6 Solving the system of equations of the stellar structure

The set of the four partial differential equations (1, 2, 17, 19) involves four dependent functions of radius and time, $m(r, t)$, $P(r, t)$, $T(r, t)$ and $L(r, t)$. If the quantities $\rho(P, T, X_i)$, ϵ , and $K_{\text{R}}(T, \rho, X_i)$ can be calculated at each position r inside the star, the system of four partial differential equations (1, 2, 17, 19) can be integrated to give the internal structure of the star at a given time, once four suitable boundary conditions are specified. Concerning the time derivative, we note that it appears explicitly in Equation (7), when the condition of hydrostatic equilibrium is violated; in the time dependence of the entropy term in Equation (20); in the equations governing the variation of the chemical abundances due to nuclear reactions and mixing. Concerning hydrostatic equilibrium we note that only in the final phases must the dynamical timescales be accounted for, or when particular effects are investigated, such as pulsations in variable stars. In all the other main phases of stellar evolution, including those of rapid contraction or expansion, the dominant timescales are much longer than the dynamical ones and the assumption of hydrostatic equilibrium is an excellent approximation. For the above reason, the entropy variation due to contraction or expansion, Equation (20), can be discretized as

$$\frac{\partial s(r, t)}{\partial t} = \frac{s(r, t_j) - s(r, t_{j-1})}{t_j - t_{j-1}}, \quad (30)$$

with t_j , and t_{j-1} being the current and the previous time step, and with all quantities at t_{j-1} being already known from the solution of the previous model.

Instead, the variation of the chemical abundance (number of atoms i per unit volume, N_i) due to nuclear reactions and/or mixing, must be explicitly followed with suitable time-dependent equations such as

$$\frac{\partial N_i}{\partial t} = \frac{\rho}{A_i \mathcal{A}} \frac{\partial X_i}{\partial t} = - \sum_j (1 + \delta_{ij}) r_{ij} + \sum_k \sum_l r_{kl,i} + \text{mixing terms}. \quad (31)$$

In Equation (31), the term r_{ij} indicates the nuclear reactions between nuclei j and i , that destroy the element i ¹² while, the term $r_{kl,i}$ refers to all the collisions between nuclei k and l that produce a new nucleus i . Here *mixing terms* refers to all other processes, besides nuclear reactions, that may change the chemical composition of a given stellar layer. The most common among such processes are convection, advection, diffusion, thermohaline mixing, and meridional circulation and shear mixing in rotating stars (see e.g. Maeder, 2009, and references therein). Usually, a homogeneous chemical composition (e.g. Asplund et al., 2021, for the solar composition), that is independent of the position within the star, is adopted for the initial model of a stellar evolution track. This is a reasonable assumption since the molecular gas out of which stars form seems well-mixed.

Opacity tables $\kappa_{\text{R}}(T, \rho, X_i)$ are provided by several authors (e.g. Iglesias and Rogers, 1996; Seaton, 2005; Hui-Bon-Hoa, 2021; Marigo et al., 2024); recent comprehensive compilations of nuclear reaction rates and resulting $\epsilon_{\text{nuc}}(T, \rho, X_i)$ are provided by Cyburt et al. (2010); Xu et al. (2013); electron neutrino energy losses, $\epsilon_{\nu}(T, \rho, X_i)$, may be found in Munakata et al. (1985); Itoh and Kohyama (1983); Haft et al. (1994), for the different processes.

3.7 Boundary conditions

Two boundary conditions can be easily derived because, at the center, $r = 0$, $L = 0$ and $m = 0$. To obtain the other two boundary conditions for P and T we need to proceed in another way. Using the results of the theory of stellar atmospheres (e.g. Mihalas, 1970) it is possible to show that, for the particular class of atmosphere models that adopt the grey Eddington approximation, the gas temperature depends on the optical depth τ in the following way:

$$T^4(\tau) = \frac{3}{4} T_{\text{eff}}^4 \left(\tau + \frac{2}{3} \right). \quad (32)$$

¹¹ $\mathcal{A} = 1/N_{\text{A}}$, where N_{A} is the Avogadro Number.

¹²When $i = j$, $1 + \delta_{ij} = 2$, because in this case two elements of type i are destroyed in each collision.

8 Evolution and final fates of low- and intermediate-mass stars

Thus T_{eff} corresponds to the physical temperature at the stellar radius R where, by definition, $\tau = \frac{2}{3}$, and the surface boundary condition for T is obtained by simply substituting T_{eff} with $T(r = R)$ in Equation (12). The boundary condition for $P(r = R)$ is obtained from the same atmosphere models, integrating the equation of the hydrostatic equilibrium from $\tau = 0$ to $\tau = \frac{2}{3}$ (Kippenhahn et al., 2013). Effects of adopting different surface boundary conditions are thoroughly discussed in literature (e.g. VandenBerg et al., 2008; Chen et al., 2014).

Early powerful numerical methods to obtain “time sequences of stellar models describing evolutionary changes” (Heney et al., 1964), i.e. stellar evolution tracks, have been developed since the middle of the last century (Heney et al., 1959; Hofmeister et al., 1964). A non-comprehensive list of popular codes to investigate stellar evolution includes ATON (Ventura et al., 2008), BASTI (Salaris et al., 2022), CESAM (Morel and Lebreton, 2008), CLES (Scuflaire et al., 2008), FRANEC (Chieffi et al., 1998), GARSTEC (Weiss and Schlattl, 2008), GENEC (Eggenberger et al., 2008), KEPLER (Weaver et al., 1978), KYP2009 (Kovetz et al., 2009), MESA (Paxton et al., 2011), PARSEC (Bressan et al., 2012), STARS (Eggleton, 1971), YREC (Demarque et al., 2008)¹³.

3.8 The Hertzsprung-Russell diagram

Once an evolutionary track is computed, its time sequence of luminosity and effective temperature are usually plotted in the Hertzsprung-Russell diagram (HRD). The HRD has been independently discovered by Ejnar Hertzsprung and Henry Norris Russell (e.g. Russell, 1914). A Colour-Magnitude diagram (CMD) is obtained if, instead of using L and T_{eff} , their observational counterparts, magnitude and colour, are adopted. To convert from an HRD to a CMD, tables of bolometric corrections are needed to translate T_{eff} , L , and surface gravity into magnitudes and colours (e.g. Chen et al., 2019). The CMD (Figure 1) and the corresponding HRD (Figure 2), are among the most useful diagnostic tools in stellar astrophysics. They inspired and guided astrophysicists in building the theory of stellar structure and evolution.

Hydrogen burning nuclear reactions

The main H burning reactions are the proton proton (PP) cycle and the Carbon, Nitrogen, Oxygen (CNO) cycle. The PP cycle is fully active at temperatures above $T \geq$ several 10^6 K and it is the typical nuclear energy generation cycle of main sequence stars with mass $M_{\text{ini}} \approx M_{\odot}$. For larger masses, when the central temperature becomes larger than about 20×10^6 K and for a non-negligible CNO abundance, the CNO becomes the more efficient cycle. Since the reaction rates of this cycle have a strong temperature dependence, the nuclear energy is produced almost entirely in the very central regions of the stars and it is transported outside by convection. Stars with $M_{\text{ini}} \leq 1.1 M_{\odot}$ (this value somewhat depending on the chemical composition) have a radiative core with a radiative temperature gradient while, stars with larger M_{ini} have a convective core with an adiabatic temperature gradient.

Proton Proton Cycle		CNO(F) Cycle	
PPI		CN	NF
$p + p \rightarrow {}^2\text{H} + e^+ + \nu$		${}^{12}\text{C} + p \rightarrow {}^{13}\text{N} + \gamma$	${}^{17}\text{O} + p \rightarrow {}^{18}\text{F} + \gamma$
$p + {}^2\text{H} \rightarrow {}^3\text{He} + \gamma$ (Low T)		${}^{13}\text{N} \rightarrow {}^{13}\text{C} + e^+ + \nu$	${}^{18}\text{F} \rightarrow {}^{18}\text{O} + e^+ + \nu$
${}^3\text{He} + {}^3\text{He} \rightarrow {}^4\text{He} + 2p$ (alt. PPII)		${}^{13}\text{C} + p \rightarrow {}^{14}\text{N} + \gamma$	${}^{18}\text{O} + p \rightarrow {}^{15}\text{N} + {}^4\text{He}$
PPII		${}^{14}\text{N} + p \rightarrow {}^{15}\text{O} + \gamma$	
${}^3\text{He} + {}^4\text{He} \rightarrow {}^7\text{Be} + \gamma$		${}^{15}\text{O} \rightarrow {}^{15}\text{N} + e^+ + \nu$	
${}^7\text{Be} + e^- \rightarrow {}^7\text{Li} + \nu$ (alt. PPIII)		${}^{15}\text{N} + p \rightarrow {}^{12}\text{C} + {}^4\text{He}$	
${}^7\text{Li} + p \rightarrow {}^4\text{He} + {}^4\text{He}$ (Low T)		ON	OF
PPIII		${}^{15}\text{N} + p \rightarrow {}^{16}\text{O} + \gamma$	${}^{18}\text{O} + p \rightarrow {}^{19}\text{F} + \gamma$
${}^7\text{Be} + p \rightarrow {}^8\text{B} + \gamma$ (Low T)		${}^{16}\text{O} + p \rightarrow {}^{17}\text{F} + \gamma$	${}^{19}\text{F} + p \rightarrow {}^{16}\text{O} + {}^4\text{He}$
${}^8\text{B} \rightarrow {}^8\text{Be} + e^+ + \nu$		${}^{17}\text{F} \rightarrow {}^{17}\text{O} + e^+ + \nu$	
${}^8\text{Be} \rightarrow {}^4\text{He} + {}^4\text{He}$		${}^{17}\text{O} + p \rightarrow {}^{14}\text{N} + {}^4\text{He}$	

In this table, p is a proton, γ a photon, e^+ a positron, ν an electron-neutrino; all other elements are indicated with their symbol and atomic weight. *alt. PPII* and *alt. PPIII* indicate the alternative branching channels through which the PP cycle of reactions may proceed further. An high order PP cycle is favored at a larger temperature and at a lower H abundance.

Low T indicates low temperature reactions that may occur already during the pre-main sequence phase, when the central temperature reaches $T = 10^6$ K. They are not energetically important, apart from the first in the list. They are relevant especially at low metallicity because at low temperatures the star is fully convective and they destroy light elements such as Deuterium, Lithium and Berillium, whose pristine abundances could be important tracers of the Big Bang Nucleo-synthesis environmental conditions.

4 Protostars and the pre-main sequence phase

Observations of stars in very young clusters, often still embedded in their parent molecular clouds, suggest that stars form in groups containing from a few thousand to many million objects. The formation involves several complex dynamical and thermal processes like self-gravity, turbulence, magnetic fields and gas heating and cooling. Altogether, these processes drive the gravitational collapse of the parent molecular clouds and their continuous fragmentation into smaller sub-units, until protostars of very low mass, $M_{\text{ini}} \leq 0.01 M_{\odot}$, are formed in their centres (Binney and Tremaine, 1987; McKee and Ostriker, 2007).

In a protostar, the inner regions reach the conditions for hydrostatic and local thermal equilibrium so that the collapse switches to a contraction. The initial protostar masses are very low, a small fraction of a solar mass, as well as their luminosity which may be less

¹³Updated or newer versions of the listed codes may be found in literature as well as other codes not in this short list.

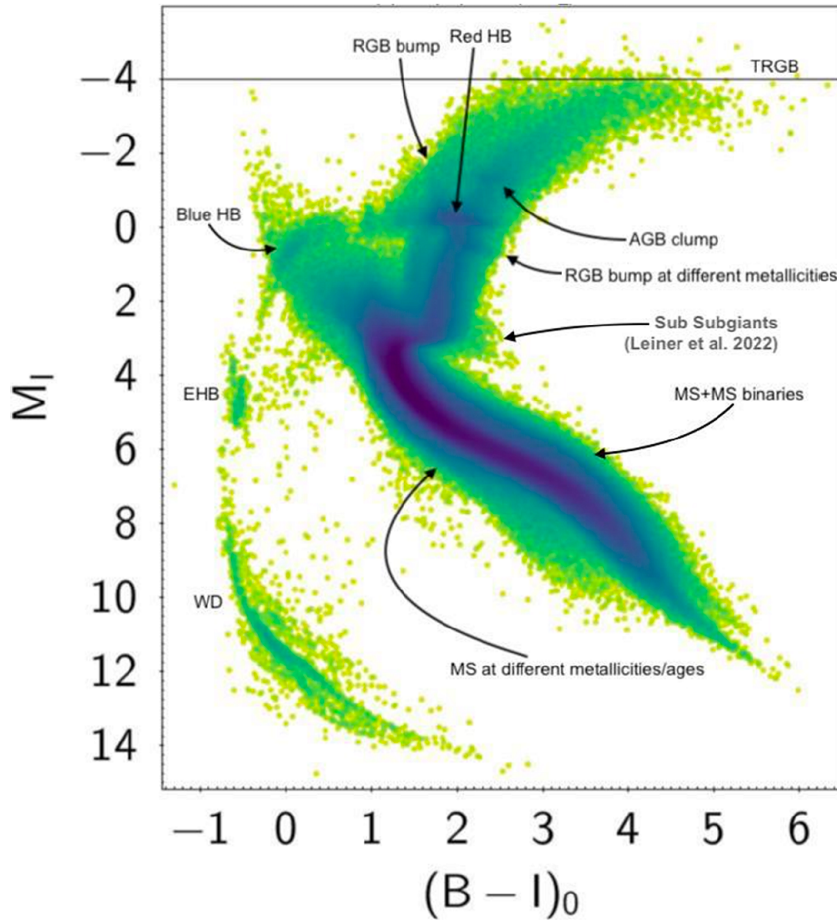


Fig. 1 The CMD of GAIA Data Release 3 stars (Credits: ESA//Gaia//DPAC - CC BY-SA 3.0 IGO. Acknowledgements: M. Bellazzini - Improvement: Marco Di Lorenzo). Stars with Galactic latitude $|b| > 50^\circ$ (Galactic Caps sample) and with relative distance error less than 10%, were extracted from the DR3 Gaia Synthetic Photometry Catalogue (GSPC). These stars are representative of different stellar populations in our Galaxy, in particular for their different initial metallicity, Z . Besides the MS of un-evolved (but nevertheless old) stars, many individual branches clearly stand out in this diagram. These indicate other important stellar evolution phases such as, SUB Giants, RGB stars and RGB bump stars, HB stars, AGB stars with AGB Bump stars and the WD stars. All these features will be discussed below.

than a thousandth of that of the Sun¹⁴. They are fully convective and they occupy a locus in the HRD representing the coolest limit for a given star mass and luminosity in hydrostatic equilibrium, the Hayashi limit (Hayashi, 1961). The internal regions quickly heat up while matter from outside continuously falls on the surface of the protostar, eventually through a rotating circumstellar disk, increasing its mass (accretion phase). When the central temperature eventually reaches values around 10^6 K, some “low temperature” nuclear reactions ignite. In such objects, the central nuclear burning of Deuterium provides enough energy to slow down the contraction and, since its abundance is continuously refueled by external accretion and convective mixing, the star has enough time to increase its mass and its luminosity (Palla and Stahler, 1993; Kunitomo et al., 2017). Once accretion ends, Deuterium is quickly destroyed and the star contracts and heats up faster. Other nuclear reactions follow, like central Li burning, but the star does not stop its contraction until the main H-burning reaction ignites. Then the star ends the pre-main sequence phase and reaches the so called Zero-Age Main Sequence (ZAMS), the starting point of evolutionary tracks plotted in Figure 2.

¹⁴An exception could be that of the very first stars in which, because of the lack of metals in the primordial gas, fragmentation could be less efficient, leading to higher protostellar masses (Klessen and Glover, 2023).

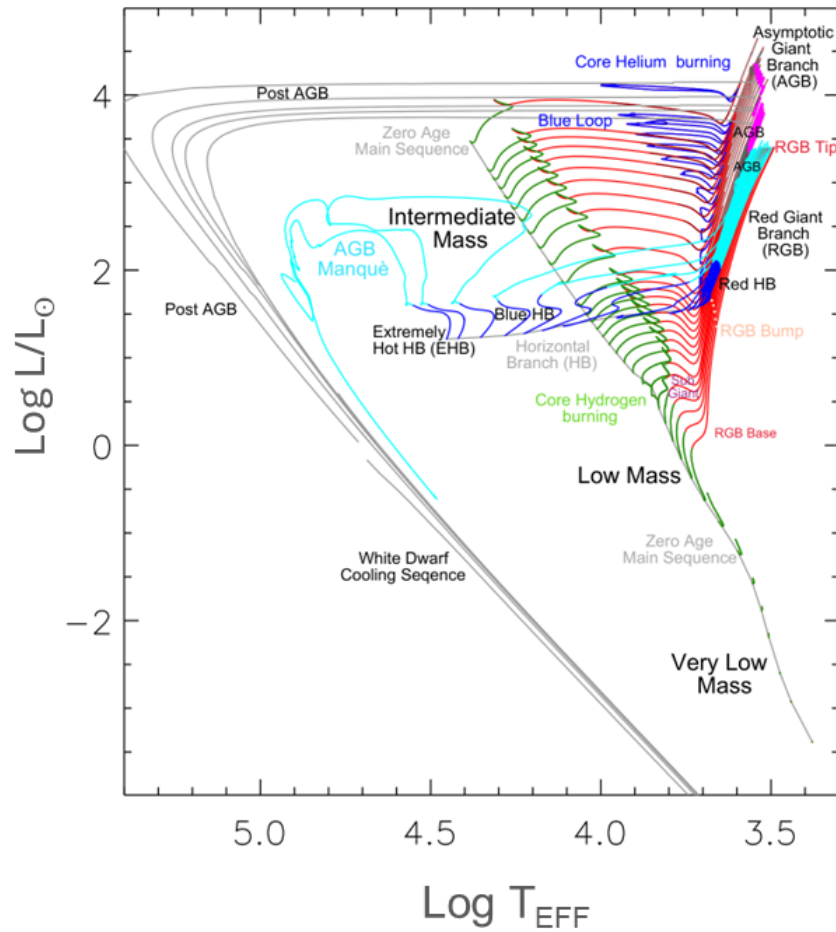


Fig. 2 A Hertzsprung-Russell Diagram of almost solar metallicity stellar evolutionary tracks at varying initial mass, with models by [Bressan et al. \(2012\)](#); [Chen et al. \(2014\)](#), [Miller Bertolami, Marcelo Miguel \(2016\)](#), for Post AGB stars) and [Salaris et al. \(2022\)](#), for White Dwarfs). This diagram is the theoretical foundation of the tools used to decipher the information contained in the CMD of Figure 1. Details on the different evolutionary phases are provided in the text.

5 The Main Sequence (MS)

The position of the observed Main Sequence of stars in the GAIA CMD is indicated by the label in Figure 1. A theoretical ZAMS is shown in Figure 2 for models of about solar metallicity. In the latter figure, the ZAMS stellar mass increases from bottom ($M_{\text{ini}} = 0.1M_{\odot}$) to top ($M_{\text{ini}} = 8M_{\odot}$). A mass luminosity relation and a T_{eff} luminosity relation are clearly seen in the HRD.

The main H-burning reactions involve the transformation of four H atoms into a He atom. The amount of energy released by each entire H fusion process can be easily calculated by considering the corresponding variation of the binding energy of the particle system, before and after the fusion. Its absolute value is obtained as the difference (e.g. Clayton, 1984)

$$\Delta E = (4m_{\text{H}} - m_{\text{He}}) c^2 \simeq 0.007 (4 m_{\text{H}} c^2) \simeq 26.732 \text{ Mev} , \quad (33)$$

where m_{H} and m_{He} are the rest masses of H and He, respectively. Equation (33) shows that the efficiency of the H fusion process is $\Delta E/4m_{\text{H}}c^2 \sim 0.7\%$. The binding energy per nucleon is computed by dividing this energy by the number of nucleons (protons and neutrons) and it is a well known function of the nucleus mass (e.g. Clayton, 1984). In spite of this very simple scheme, to account for the energy budget provided by nuclear reactions in order to follow the evolution of the star, one needs to explicitly calculate the detailed reaction rates. A non-negligible fraction of the binding energy is taken away by neutrinos when weak interactions are involved in the reactions. This is accounted for by subtracting that energy from the total budget, because the cross section of the interaction of electron-neutrinos with the plasma is so small that they freely escape from the star. Moreover one needs to account for the detailed abundance of elements, because of the explicit dependence of the reaction rates from the abundances of different isotopes.

Once such nuclear reactions are ignited in the central regions, the star reaches the so called *secular equilibrium*. Because of the strong dependence of the reaction rates on the local temperature, if the latter becomes too high, too much energy is generated and the stars expand and cool until they reach the required temperature at which the pressure gradient exactly balance the local acceleration of gravity. The opposite happens if the temperature is not sufficiently high. For the same reason, since the reaction rates depend also on the abundance of the reactants, as H is consumed the reaction rates tend to decrease, but this effect is counteracted by the contraction induced by self-gravity, that forces the star to reach the right temperature and density to maintain the hydrostatic equilibrium. Secular equilibrium is what makes a star to behave as a perfect nuclear fusion reactor, even for billions of years.

5.1 The structure of a low mass main sequence star

During the Main Sequence (MS) phase, stars convert H into He in their central regions. Their central temperature and density continue to increase slowly, of just the amount required to maintain the hydrostatic equilibrium in spite of the consumption of the reactants. This causes a secular but limited growth of their luminosity.

Throughout the duration of the MS phase, the inner region of stars with initial mass $M_{\text{ini}} \lesssim 1.1 M_{\odot}$ is stable against convection. In the outer envelope, the opacity becomes so large that the radiative gradient exceeds the adiabatic one, and convection sets in. The MS structure of stars like our Sun is constituted by a radiative core surrounded by a convective envelope. In stars with mass larger than that of the Sun, the radiation flux generated by nuclear reactions is too large to be transported by radiation alone, Equation (17). Convection is thus the most efficient way to transport energy in their central regions and the new elements produced by nuclear fusion are continuously mixed up to the border of the convective core. At the same time, a mild opacity ensures that their envelopes are radiative. The structure of such stars during the MS phase is characterized by a convective core surrounded by a radiative envelope.

While stars inhabit the MS, they obey a certain number of relationships such as the mass radius-relation, the mass-luminosity relation and the luminosity-effective temperature relation¹⁵. The latter explains why main sequence stars occupy a well defined narrow diagonal region in the colour-magnitude diagram. The mass luminosity relation of main sequence stars, which is primarily an observational fact (“...intrinsic brightness and mass are in direct relationship...” (Halm, 1911; Kuiper, 1938)) later explained by the theory, is a fundamental relation that is at the base of the *stellar evolution clock*, namely, the most common methods to measure the age of stellar systems. The typical timescale of a process involving fuel consumption is

$$\tau = \frac{E}{\dot{E}} , \quad (34)$$

where E is the energy provided by the fuel and $\dot{E} = dE/dt$ is its rate of consumption. For main sequence stars, $dE/dt = L$ and $E = QfXM$ where, Q is the amount of energy produced per gram of H that is fused, X is H abundance and fM is the fraction of the star mass that undergoes H fusion¹⁶. Thus, for the nuclear timescale one may write

$$\tau_{\text{nuc}} = \frac{QfXM}{L} . \quad (35)$$

Inserting the mass luminosity relation

$$L \propto M^{\alpha} , \quad (36)$$

¹⁵The precise form of these relationships depends on the mass range and on the chemical composition.

¹⁶ Q is almost constant while f depends on the mass of the star.

12 Evolution and final fates of low- and intermediate-mass stars

with $\alpha \sim 3.5$ ¹⁷, we get

$$\tau_{\text{nuc}} \propto QfXM^{1-\alpha} \propto M^{-2.5}. \quad (37)$$

Equation (37) shows that with increasing mass, the H-burning time decreases strongly. Since for the Sun $\tau_{\text{nuc}} \approx 10^{10}$ yr, the largest *nuclear* age of a star of solar composition is ¹⁸

$$\tau_{\text{nuc}}(M) \approx \tau_{\text{nuc}}^{\odot} \left(\frac{M}{M_{\odot}} \right)^{-2.5} \text{ yr}. \quad (38)$$

The stellar evolution clock

A stellar generation in a star cluster is assumed to be coeval and chemically homogeneous. The mass-luminosity relation forces stars of greater mass to exhaust their H fuel faster than stars of lower mass. They thus abandon the main sequence earlier, and also die earlier than less massive stars. Stars in the very upper part of an observed star cluster main sequence are those that are just abandoning it because they are just exhausting their central H fuel. Observationally, this point in the Colour Magnitude diagram is named the turn-off. The age of stars in the turn-off region, and so that of the star cluster, is equal to their H-burning lifetime, which can be obtained by models once quantities like absolute luminosity, magnitudes, colours and chemical composition are known. One of the goals of stellar evolution theory is to obtain accurate models in such a way that, when compared with observed stars, one can get their properties, in particular their age. This method has been extended to determine ages of composite stellar populations and is nowadays routinely used for determining the ages of entire galaxies up to the largest distances at very high redshift.

6 The Red Giant phase

Once H is exhausted in the center, the energy release by nuclear reactions ceases and self-gravity forces the nucleus to contract again. By applying the Virial Theorem to low- and intermediate-mass stars (Kippenhahn et al., 2013, e.g.) one may see that half of the energy produced by the gravitational contraction (E_g) is spent to increase the internal energy (E_i) to maintain the hydrostatic equilibrium, the other half being radiated away. During this phase the fuel is provided by the gravitational potential so that the typical timescale is the gravitational contraction timescale, the so called Kelvin-Helmholtz timescale (Kippenhahn et al., 2013). It corresponds to the time by which the star will lose its current internal energy with its current luminosity. Since the Virial Theorem, when applied to low- and intermediate-mass stars, states that $E_i = |E_g|/2$, we easily get that

$$\tau_{\text{KH}} = \frac{E_i}{L} \approx \frac{GM^2}{2RL}. \quad (39)$$

6.1 The Sub-giant branch (SGB)

For the Sun, $\tau_{\text{KH}} \approx 3.1 \times 10^7$ yr, which is much shorter than τ_{nuc} but much larger than τ_{dyn} . So, during the contraction phase the stars maintain the hydrostatic equilibrium. The contraction of the H exhausted core increases the temperature of the surrounding H-rich regions until, very quickly, H burning ignites there. At this point the star is constituted by a nuclear inert He core surrounded by a H-rich envelope, at the base of which a shell of H-fusion converts H into He. As the time elapses, the temperature and density of the He core increase while the shell feeds new He to the central nucleus. The higher the core temperature, the larger the H nuclear reaction rates in the shell and the luminosity they provide. This produces an expansion of the H-rich envelope with an initial fast growth of the radius. The surface of the star cools while its size becomes larger and larger. Initially the envelope is radiative and the excess luminosity causes a strong expansion. In the HRD, the star moves at almost constant luminosity toward the Hayashi limit at lower effective temperatures (the Sub Giant Branch, SGB). As the external envelope cools, the opacity increases, because a larger fraction of the envelope enters the temperature region where H and He partially recombine, where opacity shows a large peak. The convective envelope begins to penetrate into deeper regions than during the previous H-burning phase. Convection is very efficient and it is able to transport all the luminosity from its base to its surface with an adiabatic temperature gradient, without causing a significant expansion. Once convection reaches the central H-poor regions all the luminosity produced by the inner H-burning shell is transported outside without any further expansion. At this point, the path of the star in the HRD turns from horizontal to almost vertical and the excess luminosity generated by the shell is immediately shown at the stellar surface. This turning point defines the base of the Red Giant Branch (RGB) and it is clearly seen in the CMD of well populated star clusters. For the solar model this happens when the convective envelope reaches the inner 50% of the mass. Needless to say that the effective temperature of this point in the HR diagram depends critically on the ML parameter that determines the efficiency of the convective energy transport. It is interesting to note that with the MLT calibration obtained from the Solar model, the theory is also able to reproduce

¹⁷The exponent α depends on the stellar mass because of the different efficiency of nuclear reactions and of the different opacities. It decreases toward more massive stars and also toward lower mass stars.

¹⁸This is only a rough approximation assuming that the quantities f, α, X do not change. Moreover the H-burning time is taken as the total *nuclear* time of a star because further nuclear reactions are significantly less efficient than H-burning and because these generally occur at a higher luminosity. In astrophysical studies the total time is always computed accounting for all the processes.

the observed location of the base of the RGB in the observed CMD of many star clusters¹⁹.

6.2 The Red Giant Branch (RGB)

At the beginning of the SGB phase, the He core mass of a solar mass star is only $0.019 M_{\odot}$ with a central density of 1000 g cm^{-3} and a central temperature 20 million K. At the end of the SGB phase, the He core mass reaches $0.130 M_{\odot}$, with a central density of 30000 g cm^{-3} and a central temperature of 26 million K. However the temperature needed for the ignition of the next nuclear fuel, He, under normal conditions is of about 100 million K.

Degeneracy of stellar matter

Electron Degeneracy in Stars

In the limiting case of a totally degenerate gas of electrons the equation of state for the non relativistic limit is (Kippenhahn et al., 2013)

$$P = \frac{8\pi}{14h^3 m_e} \left(\frac{3h^3}{8\pi\mathcal{A}} \right)^{5/3} (\rho/\mu_e)^{5/3} \approx 9.99 \times 10^{12} (\rho/\mu_e)^{5/3}, \quad (40)$$

where one should use Equation (26) for μ_e . At increasing density, electrons will become relativistic. For a totally degenerate gas of relativistic electrons the pressure is (Kippenhahn et al., 2013)

$$P = \frac{hc}{8\mathcal{A}} \left(\frac{3}{\pi\mathcal{A}} \right)^{1/3} (\rho/\mu_e)^{4/3} \approx 1.243 \times 10^{15} (\rho/\mu_e)^{4/3}. \quad (41)$$

The mass radius relation of degenerate stars and the Chandrasekhar mass limit

Considering only electron pressure and combining Equation (40) for a completely degenerate non relativistic configuration with the hydrostatic equilibrium condition Equation (3), we may obtain a relation between the total mass and surface radius

$$\begin{aligned} 9.99 \times 10^{12} (\rho/\mu_e)^{5/3} &\approx 0.5 \frac{GM^2}{4\pi R^4} \\ 9.18 \times 10^{11} \frac{M^{5/3}}{R^3 \mu_e^{5/3}} &\approx 0.5 \frac{GM^2}{4\pi R^4} \\ \left(\frac{M}{M_{\odot}} \right)^{1/3} \frac{R}{R_{\odot}} \left(\frac{\mu_e}{2} \right)^{5/3} &= 0.0123. \end{aligned} \quad (42)$$

This is the mass-radius relation for degenerate configurations, like the inner He core of a RGB star. At increasing mass, the radius decreases and the density increases further. At a certain density electrons become relativistic. In the limiting case of relativistic complete degeneracy, after combining Equation (41) with the hydrostatic equilibrium condition Equation (3), the dependence on the radius vanishes and we obtain a constant value for the mass

$$M_{\text{Ch}} = \left(\frac{hc}{8\mathcal{A}G} \right)^{3/2} \frac{3}{\pi\mathcal{A}} \frac{1}{\mu_e^2} \sim \frac{5.836}{\mu_e^2} M_{\odot}. \quad (43)$$

This value was obtained for the first time by Chandrasekhar (1935) who discovered that there is a limiting configuration above which totally electron degenerate stars can no longer fulfill the hydrostatic equilibrium condition, possibly leading to a collapse of the compact object. In the case of a mixture without H (He core or CO core) $\mu_e \approx 2$ and $M_{\text{Ch}} \approx 1.459 M_{\odot}$. For Iron, $\mu_e \approx 2.15$ and $M_{\text{Ch}} \approx 1.263 M_{\odot}$.

The plasma is almost fully ionized and free electrons move with an average kinetic energy which is equal to that of the nuclei (i.e. $E_k = 3/2 k_B T$), following the energy equipartition principle. Another consequence of the Virial Theorem is that, in a contracting core the central values of ρ and T follow the relation

$$\rho_c \propto T_c^3. \quad (44)$$

However, as the matter density increases, the electron gas may become more and more degenerate as a consequence of the Pauli exclusion principle for fermions (Pauli, 1925). Indeed, by comparing Equation (40) with the EOS of a non-degenerate ideal gas of electrons, $P_e = \rho k_B T / \mu_e \mathcal{A}$, we see that the limit where the contribution of degenerate non relativistic gas exceeds that of non-degenerate electron gas occurs when the density, at a given temperature, exceeds the threshold established by the following relation

$$\rho_c \propto T_c^{3/2}. \quad (45)$$

Equation (45) runs flatter than Equation (44) and the point of their intersection depends on the mass of the contracting core. Low mass stars are, by definition, those stars for which the intersection of Equation (44) and Equation (45) happens before reaching the temperature for He ignition, implying that their contracting He nuclei become electron degenerate before they are able to ignite He. Because of the exclusion principle, in a fully degenerate gas of electrons all the momentum states are occupied up to a threshold value, and new electrons that can be confined in the same elemental volume must occupy higher momentum (energy) states. The electron gas becomes more and more difficult to compress and the equation of state need to account for this effect. Protons and neutrons too obey the same principle but the density at which they begin to be affected is much higher than that of electrons. Thus, while for non-degenerate ions the average

¹⁹However, there is increasing evidence, also from hydrodynamic models of stellar convection, that the MLT parameter may slightly depend on the stellar parameters (Trampedach et al., 2014).

kinetic energy per particle continues to be a function of the temperature ($3/2 k_B T$), for the degenerate electrons it becomes progressively higher than that, and more and more dependent on the matter density. The velocities of the electrons become progressively higher at higher densities, their mean free path becomes also higher, and electron conduction may become the most efficient energy transport mechanism, producing large isothermal regions in the deep interiors. The gas remains ideal (only particle collisions are considered) but the equipartition of energy between ions and electrons ceases to hold: electrons acquire an average energy that is several times larger than $3/2 k_B T$. The gravitational energy of the contraction goes mainly into increasing the electron energy and not that of the ions (their temperature) and the equation of state becomes less and less dependent from the temperature.

If, for some reason, the Sun were to instantly lose its H-rich envelope and remain with an He core of $0.130 M_\odot$, it would evolve in the following way²⁰. The contraction would increase its density until it would become totally degenerate; the whole core will eventually become almost isothermal; energy will be continuously lost by radiation driving the object toward a low luminosity cooling phase that could last for an indefinite time. This will be a prototype of a He White Dwarf. However, single stars that reach the RGB phase in less than a Hubble time, must have a large H-rich envelope²¹. The presence of such H-rich envelope completely changes the subsequent evolution. The H-burning shell at the bottom of the envelope continuously feeds fresh non-degenerate He particles to the electron degenerate He core. While the mass of the He core grows, its average density and temperature increase, in particular that of the non-degenerate gas of He nuclei. The luminosity and radius of the star increases while, in the HR diagram, the stars climb along the so called Red Giant Branch. The driving mechanism of the evolution is the outward (mass) displacement of the H-burning shell, that occurs in a nuclear timescale. For this reason the Red Giant Branch of low mass stars is well populated, as can be seen in the CMD of many globular clusters (GCs).

During the ascent on the RGB, many physical processes occur that may leave important observable features. Just after the RGB base, the convective envelope deepens down to about the inner 20% of the total star mass. After that point, the structure of the star is well described by an inner electron-degenerate He core, surrounded by a very thin H-burning shell on top of which there is an extended H-rich convective envelope that reaches the photosphere. The chemical composition within the envelope is almost homogeneous and all the differences between regions that were, or were not, altered by nuclear H fusion in the previous phases, are erased. Convection transports the traces of inner material that were processed by CNO nuclear reactions to the surface (First Dredge-Up phase). One such feature is the conversion of almost all C into N and the other one is the $^{12}\text{C}/^{13}\text{C}$ isotopic ratio that, from an initial value of about 100, is reduced by at least a factor 10. Another feature is the larger He content in the internal regions. What we see at the surface is the result of the dilution of the internal nuclear processed material with the more external original composition²². The outward speed of the H-burning shell depends on its temperature and density conditions and on its H abundance. In a well populated star cluster, the observed number of stars at any luminosity (luminosity function) along the RGB, together with their effective temperature and their surface chemical composition, can be compared with what predicted by models. In this way we may test the robustness of the physical ingredients that we are using in the models, including nuclear reaction rates, neutrino emission processes, opacity of stellar matter, equation of state, convection theory, efficiency of mixing and even assumptions in the numerical procedures²³. For example, when the H-burning shell reaches the border left by the maximum penetration of external convection it finds a steep H profile. At this point, the star spends a certain time to readjust its thermal equilibrium to the higher H abundance of the burning shell. The excess time spent results in a clearly detectable excess of the number of stars in that particular point along the RGB, that is known as the RGB Bump. As the He core mass grows, the luminosity and the radius of RGB stars increase. They may reach a luminosity that is 2500 times larger than that of the Sun and a radius that is comparable to the Earth's orbit. Since these high luminosities allow them to be observed even in external galaxies, these stars have been and are the subject of countless astrophysical investigations (e.g. [Freedman and Madore, 2010](#), and citing papers).

6.3 The Tip of the Red Giant Branch (TRGB)

When the He core approaches a mass $M_{\text{He}} \sim 0.5M_\odot$, the inner temperature reaches a value around 10^8 K, which is high enough to cause a relevant fusion of pairs of He nuclei into ^8Be . The resulting excited ^8Be nucleus rapidly decays in its most likely channel $^8\text{Be} \rightarrow ^4\text{He} + ^4\text{He}$ giving rise to only a trace of ^8Be equilibrium abundance²⁴. However at a density of more than 10^5g cm^{-3} and a temperature of $\sim 10^8$ K the production of C by the α capture reaction $^8\text{Be} + ^4\text{He} \rightarrow ^{12}\text{C} + \gamma$ becomes relevant. Since this fusion of three He nuclei into ^{12}C happens almost simultaneously, this process is named the *triple- α* nuclear burning process.

In the case of secular equilibrium, an excess of nuclear energy production increases the local temperature that immediately increases the pressure, forcing the surrounding matter to expand and cool to restore an equilibrium condition. The ignition of the 3α nuclear reactions in a star climbing the RGB happens inside a strongly electron degenerate core, for which the dependence of the EOS from the temperature is negligible, $\partial \ln P / \partial \ln T \approx 0$ (see also Equation (40) and Equation (41)). The excess temperature does not produce a local expansion. Instead the local temperature increases, strongly increasing the local release of heat (photons). This cycle might be explosive and, since it should

²⁰A scenario of this kind could be the result of tight binary evolution. The more massive component is a low mass stars that evolves away from the Main Sequence. While in the SGB or RGB, it fills its Roche Lobe and it is spoiled of its H-rich envelope that is partially or totally accreted by the secondary star, which is less massive and still on the main sequence.

²¹The oldest stars with initial mass $M_{\text{ini}} \leq 0.85M_\odot$ have a H-burning lifetime t_{H} larger than the Hubble time $t_{\text{Hub}} \approx 13.7\text{Gyr}$, and so they should still populate the MS.

²²There is also evidence that, besides the RGB dilution, some other mixing mechanism is active, such as thermohaline mixing ([Charbonnel, C. and Zahn, J.-P., 2007](#)).

²³Effects of interactions with some still unknown type dark matter have also been tested using RGB observations ([Raffelt and Weiss, 1995](#); [Straniero et al., 2020](#)).

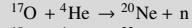
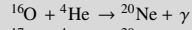
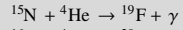
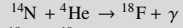
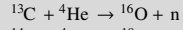
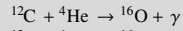
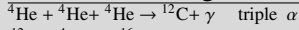
²⁴This is the reason why the Big Bang nucleosynthesis could not proceed beyond He and produced only traces of Li and Be ([Cyburt et al., 2016](#)).

ignite near the center of the star²⁵, it could easily destroy the entire star. However the ignition region is not totally degenerate and convection and conduction drive heat toward less dense regions where electron degeneracy is even less. Thus, in a very short time-scale, the 3α nuclear reactions produce a strong energy release that is able to expand the surrounding layers, decreasing the degeneracy of electrons until further nuclear burning becomes stable. About 5% of He is transformed into ^{12}C during this so called He-Flash. Correspondingly, the envelope undergoes a strong contraction and, in the HRD, the star moves from the Tip of the RGB (TRGB) to a lower luminosity and a hotter effective temperature, the so called Horizontal Branch (HB).

Main Helium-burning nuclear reactions

The main He-burning reactions in low- and intermediate-mass stars are summarized below.

Helium-Burning Reactions



Reactions with elements of higher atomic number generally require higher temperatures and, in low mass stars, the rates for reactions that go beyond ^{16}O are negligible. Since the α capture reactions have a strong temperature dependence, the nuclear energy during the main He-burning phase is produced almost entirely in the very central regions and it is transported outside by convection. During central He-burning all stars have a convective core with an adiabatic temperature gradient.

The Helium Flash

The He-flash is a characteristic of all stars with initial mass between $0.5M_{\odot}$ and about $M_{\text{Flash}} \approx 2.0M_{\odot}$. The precise value of M_{Flash} depends on other physical stellar parameters like chemical composition and efficiency of mixing. In this mass range, electrons in the central regions become strongly degenerate after central H-burning phase. Stars below $0.5M_{\odot}$ may also become degenerate but they will not be able to reach the temperature for He ignition (100 million K). During the contraction, stars with higher mass evolve at a higher temperature and lower density, so that stars with $M_{\text{ini}} \geq M_{\text{Flash}}$ are able to quickly contract to the He ignition temperature, with a density that never reaches the limit for strong electron degeneracy. This characteristic is adopted to separate low- and intermediate-mass stars. Electron degeneracy is also able to prevent H ignition in very low mass stars. Indeed stars with mass below $0.08M_{\odot}$ are not able to ignite H after their pre-main sequence phase and become H Dwarfs that, for their lower surface temperature, are named Brown Dwarfs.

7 The Horizontal Branch (HB)

The HB is the locus of the HRD where low mass stars burn He in their center. Its name is due to the fact that, using the bolometric magnitude²⁶, it appears to be almost horizontal in the middle of the CMD, sometimes extending from the RGB to beyond the MS. To understand the almost constant luminosity of the HB it is enough to consider that all the RGB stars need to reach almost the same He core mass $M_{\text{He}} \sim 0.5M_{\odot}$, to ignite the 3α reactions. Since the luminosity on the HB is mainly due to the He-burning reactions, they have almost the same luminosity. HB stars with different initial mass have different envelope mass. The greater the envelope mass, the larger its total opacity, and the redder the corresponding effective temperature in the HRD. Old Open Clusters have turn-off masses $M_{\text{ini}} \sim 1.5M_{\odot}$ and, since $M_{\text{He}} \sim 0.5M_{\odot}$, the envelope mass of their He-burning stars are quite large. They thus populate the red region of the HB, the Red-HB. For field low mass stars this region is also named the Red Clump (Girardi, 2016). Turn-off masses of galactic GCs are around $0.85M_{\odot}$ and their envelope mass should be $\sim 0.35M_{\odot}$, which still produces a too high opacity to allow the star to populate the Blue-HB side. In order to occupy the Blue-HB, seen in many GCs, stars must have envelopes of a significantly lower mass. The common view is that old evolved low mass stars lose a significant fraction of their mass ($\sim 0.2M_{\odot}$) while ascending the RGB (Reimers, 1975, 1977; Fusi-Pecci and Renzini, 1975; Schröder and Cuntz, 2005).

While RGB mass loss could explain the presence of different HB morphologies (Blue or Red-HB) in different GCs, either by means of age differences (older GCs have lower turn-off masses and should appear hotter), or by metallicity differences (more metal-poor GCs have lower envelope opacities and should be hotter), it is really challenging to explain a composite morphology (Blue and Red-HB) in the same GC, as often observed. In fact, there is growing evidence that, contrary to what believed in the past, many galactic and also extragalactic GCs are not homogeneous stellar systems but show correlated differences in chemical composition, e.g. Oxygen, Sodium, Aluminum, indicating the presence of multiple stellar generations (Milone and Marino, 2022). Particularly relevant to determine the HB morphology is

²⁵At the central temperature and density a certain fraction of electron neutrino/antineutrino pairs are produced that are able to cool the more internal regions and shift the maximum temperature slightly off-center.

²⁶The bolometric magnitude measures the luminosity in the whole spectral range. Standard magnitudes, instead, measure the flux received in a relatively narrow range of frequencies, losing the photons that falls outside this range.

the initial He content of different generations, which has been found to vary, in the same GC, by $\delta Y \sim 0.10$ to $\delta Y \sim 0.15$ with respect the cosmological nucleosynthesis value (Pasquini, L. et al., 2011; Marino et al., 2013). A large surface He content may give rise to a Blue-HB and even to an Extreme (hot) HB (EHB), even at high metallicity (Bressan et al., 1994). The reason of this large He spread at a very low metallicity is still under debate (Milone and Marino, 2022).

Stellar Mass loss

Mass-loss is a mechanism by which a star loses mass during its evolution. For the Sun, the current mass loss rate is estimated to be $\dot{M} \sim 3 \times 10^{-14} M_{\odot} \text{ yr}^{-1}$. Since its H-burning lifetime is estimated to be $t_{\text{H}_0} \sim 10 \times 10^9 \text{ yr}$, the total mass lost at this rate would be negligible ($\sim 0.0003 M_{\odot}$). In other stars mass loss may be larger, e.g. old GCs stars loose about 20% of their initial mass while climbing the RGB. Or even dramatic as in high metallicity supergiant stars, that may lose more than 80% of their initial mass before dying (Vink, 2022). Mass loss is another important but uncertain process in stellar evolution.

8 Intermediate mass stars

Stars more massive than $M_{\text{ini}} \geq M_{\text{Flash}}$ have a main sequence evolution that is very similar to that of the upper range of low mass stars. This is because, in both cases, H is burnt in a convective core (i.e. through the CNO cycle). The main sequence mass-luminosity relation implies that their typical H-burning lifetimes are shorter than those of low mass stars, spanning from one billion years to hundreds of millions of years for intermediate mass stars, and reaching a few million years in massive stars. A formal separation between intermediate and massive stars is set at $M_{\text{ini}} = M_{\text{AGB}} \sim 8 M_{\odot}$, due to the different post-main sequence evolution of stars in the two mass ranges. The value of M_{AGB} depends from several parameters, the most important ones being the elemental abundance and the mixing efficiency of internal convection and, eventually, of rotation. After the main sequence phase, the He core of stars more massive than $M_{\text{ini}} \geq M_{\text{Flash}}$ contracts and quickly reaches central temperatures in excess of 100 million K, at which stage the triple- α process begins. The typical time scale of the contraction phase, the Kelvin-Helmholtz timescale, is much shorter than the nuclear time scale and, since the observed number of stars in any post main sequence phase is proportional to the duration of the phase, only very populous clusters show stars in this phase of their CMD. In galactic Open Clusters, for example, it is unlikely to observe stars in this contraction phase. During this fast contraction, the H-burning shell has no time to significantly increase the mass of the He core, and the luminosity of the Red Giant Branch at central He ignition, is not much higher than that at the end of the MS. These stars have large convective envelopes and their central He-burning ignites and continues burning in the hotter side of their RGB. In the main central He-burning phase, the total luminosity is also partly provided by the H-burning shell. Depending on the relative intensity of the He and H nuclear energy sources, the star may either continue and conclude its He-burning phase near the RGB or, after a certain time that depends on other physical parameters²⁷, it may quickly move toward the MS, continuing the core He-burning phase as a Blue/Yellow Giant star. The star performs a Blue Loop in the HR and, for this reason, stars in this phase are named Blue Loop Stars. During this loop the star may cross the Cepheid Instability Strip. Inside this strip the envelope becomes dynamically unstable and the star may undergo periodic radial oscillations. Given the dynamical nature of this instability these stars show a well defined Period-Luminosity relation (Leavitt and Pickering, 1912) that constitutes a fundamental milestone for astronomical distance determinations and, as such, a milestone for our understanding of the geometry of the Universe.

The period luminosity relation of variable stars.

Starting from Equation (9) and eliminating the radius using the definition of the effective temperature, $L = 4\pi R^2 \sigma T_{\text{eff}}^4$ we obtain for the dynamical timescale \mathcal{P}

$$\mathcal{P}^2 = \frac{R^3}{fGM} = \frac{1}{fGMT_{\text{eff}}^6} \left(\frac{L}{4\pi\sigma} \right)^{\frac{3}{2}}. \quad (46)$$

Equation (46) shows that variable stars located within a region of dynamical instability in the HRD follow a characteristic relationship between the period of the instability and the total mass, the surface luminosity and the effective temperature. One of such regions is the Cepheid instability strip, from the name of the prototype of this class of stars, Delta Cephei. Since this strip is quite narrow and almost vertical in the HR diagram, while the blue loops are almost horizontal and with a well defined mass-luminosity relation $L = L(M)$, this relation becomes a period-luminosity relation, see (e.g. Ripepi et al., 2019).

$$\log_{10} \mathcal{P} = \alpha(M, T_{\text{eff}}) + \beta \log_{10} L. \quad (47)$$

Another similar class is that of RR-Lyrae variables, that are located at the crossing of the instability strip with the HB in GCs (Marconi et al., 2015). An overview of the different classes of variable stars across the HRD can be found in Eyer and Mowlavi (2008).

²⁷Chemical composition, mixing efficiency, efficiency of different He nuclear reaction rates and opacity.

9 Final nuclear phases of low- and intermediate-mass stars

After central He exhaustion, low- and intermediate-mass stars have a very similar fate. Their structure consists of a central core, composed mainly of C and O (CO core), surrounded by an extended He-rich zone (the fraction of the previous He core above the central convective region) and an external H-rich envelope. The CO core contracts and heats up, going toward the ignition of the next nuclear fuel of C, at about 7×10^8 K. Because of heating produced by contraction, He-burning continues in a shell just above the CO core. The luminosity produced by both contraction and nuclear reactions expands and cools the whole envelope. In the HRD the stars move asymptotically toward the Red Giant Branch with increasing luminosity and decreasing effective temperature. For this reason the following phase is named the Asymptotic Giant Branch.

9.1 The Asymptotic Giant Branch

Neutrino energy losses.

Weak interactions theory predicts that, instead of an electromagnetic interaction emitting a photon (γ), an electron neutrino-antineutrino pair ($\nu\bar{\nu}$) is created with a very small relative probability, ρ , given by

$$\frac{\rho(\nu\bar{\nu})}{\rho(\gamma)} \simeq 3 \times 10^{-18} \left(\frac{E_\nu}{m_e c^2} \right)^4, \quad (48)$$

where E_ν , the neutrino energy, is typically of the order of the average electron energy, $\sim k_B T$ or even larger in degenerate matter (e.g. [Maeder, 2009](#)). The neutrino cross section under usual stellar conditions is so small, $\sigma_\nu \sim 10^{-44} \text{cm}^2$, that the neutrino's mean free path is $l_\nu \simeq 1/(n_e \sigma_\nu) \simeq 10^{20} \text{cm}$. Since the mean free path of photons in a dense stellar plasma is of the order of a centimeter, under certain conditions the number of electromagnetic interactions is so high that, in spite of its very small relative probability, the $\nu\bar{\nu}$ process becomes a significant sink of energy. The high temperature dependence implied both by the right hand side term in Equation (48) and by the energy density of photons ($\propto T^4$) indicates that neutrino losses strongly increase with the temperature. Electron neutrino pairs, $\nu\bar{\nu}$, can be produced instead of electron scattering interactions, free-free (Bremsstrahlung) interactions, electron-positron pair production and plasmon production ([Haft et al., 1994](#)).

As the CO core contracts, the central temperature and density increase reaching typical values of $T_c \simeq 2 \times 10^8$ K and $\rho_c \geq 10^5 \text{g cm}^{-3}$, where neutrino losses become important. The energy released by gravitational contraction is consumed by neutrinos, thus preventing further heating of the core that enters a phase of strong electron degeneracy. This fate is common to both low mass stars that undergo the He-flash, and to intermediate mass stars that ignite He in a non degenerate gas, up to an upper mass limit $M_{\text{AGB}} \simeq 8M_\odot$.

During the early stages (Early Asymptotic Giant Branch) the He shell quickly moves outward approaching the H shell, that is temporarily extinguished by the expansion and cooling of the envelope. Envelope convection deepens and, in more massive AGB stars, penetrates into the underlying He-rich layers, pushing the bottom of the H-rich envelope toward the He-rich core. He and N produced by previous H-burning phase are thus transported to the surface (second Dredge-up phase). In a time scale that may last about one tenth of the central He-burning phase the He-burning shell reaches the base of the H-rich envelope, thus providing enough heating to reignite the H shell. At this point, the He shell quenches off and the star enters the Double Shell Phase (H and He), proceeding with a series of intermittent and alternate ignitions of the H and He shells ([Iben and Renzini, 1983](#)). H-shell burning increases the intermediate quiescent He-rich region; when the latter reaches a certain mass threshold the He-shell ignites via the triple- α process; ignition is abrupt because heat cannot be efficiently transported away (He thermal pulse), not even by convection that engulfs the He-rich intermediate region with the newly generated C. Ultimately, the heat wave reaches the bottom of the H-rich envelope causing a strong expansion and the quenching of both the H and He shells. The external convection may penetrate into the He-rich region giving rise to the Third Dredge-up phase during which further He-rich matter is conveyed to the surface. In some cases the surface is also enriched by ^{12}C freshly produced during the thermal pulse. Once the heat wave is completely absorbed by the external envelope the latter contracts and the H shell ignites again, lasting for most of the time (interpulse period), until a further thermal pulse occurs after a thousand or tens of thousands of years ([Herwig, 2005](#))²⁸. The combined effect of the alternate H-and He-shell burning is that the mass of the degenerate CO core, M_{CO} , increases toward M_{Ch} which, for a CO-rich composition is of about $1.4M_\odot$. However, observations and current models suggest that AGB stars lose their whole H-rich envelope before M_{CO} reaches M_{Ch} . On one side there are observations suggesting the presence of strong matter outflows leaving the stars at high rates, several $10^{-5} M_\odot \text{yr}^{-1}$ ([Goldman et al., 2017](#); [Homan et al., 2018](#)). These high mass loss rates may evaporate an envelope of $5 M_\odot$ in a time scale of a few 10^5 yr, which is much shorter than the nuclear timescale needed for the H- and He-burning shells to increase the core mass to the Chandrasekhar limit ([Marigo et al., 2008](#)). The other key evidence is the so called White Dwarfs initial-final mass relation showing that the progenitors of observed White Dwarfs ($0.55M_\odot \lesssim M_{\text{WD}} \lesssim 1.2M_\odot$) are low- and intermediate-mass stars with $0.8M_\odot \lesssim M_{\text{ini}} \lesssim 7M_\odot$ ([Cummings et al., 2018](#); [Marigo et al., 2020](#); [Addari et al., 2024](#)).

9.2 The Post Asymptotic Giant Branch

While stars ascend the AGB, their envelope is removed by strong mass loss. Once the envelope mass is reduced to a few thousandths of a M_\odot , the surface temperature begins to increase and the star leaves the AGB. The H-burning shell and the weaker but still efficient mass

²⁸A series of III Dredge-Up episodes may significantly increase the surface ^{12}C abundance in such a way that the number abundance ratio $^{12}\text{C}/^{16}\text{O} > 1$. Then, the star appears as a C-(spectral) type star, in net contrast to M-type giants that show $^{12}\text{C}/^{16}\text{O} < 1$. When the ratio $^{12}\text{C}/^{16}\text{O} \simeq 1$, the star is of spectral type S.

loss are able to consume/remove the residual H envelope and the star exposes its naked internal core. When its surface temperature reaches 30000 K the photosphere begins to emit energetic photons that are able to ionize the circum-stellar gas previously lost. The stars assume the characteristic morphology of Planetary Nebulae: nebulae that are ionized by a central source, which are among the most beautiful extended objects that can be observed in the sky, an example is shown in Figure 3. The life of these objects is relatively short because their circum-stellar gas is quickly swept away by radiation pressure and at the same time, the central star begins its cooling phase toward the White Dwarf stage (Miller Bertolami, Marcelo Miguel, 2016).

Stars with initial mass in a narrow mass range $M_{AGB} \leq M_{ini} \leq M_{SAGB} \approx M_{AGB} + 2M_{\odot}$, are able to ignite the $^{12}\text{C}+^{12}\text{C}$ reaction without experiencing strong electron degeneracy in their CO cores. They produce a ^{12}C exhausted Oxygen/Neon-rich core, that contracts and evolves toward strong degeneracy. These stars experience a similar final evolution toward the AGB phase but, being more massive and luminous, they are named Super-AGB stars (Siess, 2007).



Fig. 3 The Ring Nebula (Credits: ESA/Webb, NASA, CSA, M. Barlow (UCL), N. Cox (ACRI-ST), R. Wesson (Cardiff University) and STScI CC BY-SA 3.0 IGO. The Ring Nebula (also known as M57 and NGC 6720) captured by the James Webb Space Telescope (JWST). The planetary nebula is located about 2,500 ly away in the constellation Lyra, and is formed from a dying low-mass star expelling its outer layers. The ring structure and colors display ionized gas which is illuminated by the central star. The post-AGB central star has a mass $M \approx 0.61 - 0.62 M_{\odot}$ and primarily composed of C and O, with a surface $T_{\text{eff},*} \approx 120,000 \text{ K}$ and luminosity $L_* \approx 200 L_{\odot}$ (O'Dell et al., 2007), indicating the star is now approaching the WD cooling sequence.

10 White Dwarfs

White Dwarfs are thought to be the most common evolved stars because, on one side, all stars with mass $M_{ini} \leq M_{SAGB}$ will sooner or later end their nuclear life in that way and, on the other, the lifetime of the WD phase may be even larger than the Hubble time. In the HR diagram, the WD sequence is located on the left (hotter) of the MS, with a luminosity and an effective temperature that decrease almost parallel with that of the MS. However, the higher temperature at any given luminosity suggests that WDs have radii about one hundredth that of a MS star. For a similar mass, this implies a volume that is a millionth, and a density that is a million times that of a MS star with a similar

luminosity, respectively. This simple argument discloses the power of a well done HR diagram. Since the early theoretical interpretations of WDs, it was clear that they must have a very high central density. Indeed, the fact that a WD must be supported by strongly degenerate electrons (Fowler, 1926) is considered the first application of the Pauli exclusion principle (Kaplan, 2020).

A completely degenerate configuration is a very good approximation for WDs, implying that they follow an inverse mass radius relation Equation (42), and that there is an asymptotic upper mass limit, M_{Ch} , above which they cannot be kept in hydrostatic equilibrium, (see Equation 43). For He- or CO-WDs, $\mu_e \sim 2/(1+X) = 2$ and so $M_{\text{Ch}} \sim 1.46M_{\odot}$ ²⁹. During the Post-AGB phase, the star quickly crosses the HRD from the coolest to the hottest regions, reaching T_{eff} larger than ~ 100000 K. Then, once nuclear energy generation from the outer very thin H-shell quenches off, the star begins to cool again. In this phase, most of the cooling is due to electron-neutrino production by weak interaction from the deep interiors. After a few tens of Myr the interior temperature is no longer high enough for efficient production of neutrinos, and cooling slows down. T_{eff} is now below 30000 K and further luminosity is provided by internal readjustment of the ions gas. At increasing density and decreasing temperature, electrostatic interactions become more and more competitive with respect to the thermal energy and force ions, that continue to be non-degenerate, to change from an almost perfect gas phase to liquid and, ultimately, to solid phases. This crystallization process lasts for billions of years. Because of the inverse mass-radius relation, density is higher in more massive objects so that they begin this process earlier and proceed faster, at least in the early stages. While the above processes may provide the fuel, the cooling rate is actually governed by the transport mechanisms across a thin external envelope that, because of its opacity, acts as thermal insulator (e.g. Saumon et al., 2022). The interior regions are kept almost isothermal by the large mean free path of degenerate electrons³⁰. Recent cooling tracks for WD stars can be found in Saumon et al. (2022); Salaris et al. (2022). Comparing the observed WD sequences in stellar systems with their theoretical counterparts is a powerful independent method to estimate their age (Qiu et al., 2021; Tononi et al., 2019; Campos et al., 2016; Bergeron et al., 1997). However the rate at which WD cool down, and the corresponding location in the cooling sequence of the HR diagram, depend strongly on the exact balance between the sources of energy and the efficiency of energy transport at the stellar photosphere, and this may introduce some uncertainties, especially in the timescales of the process (see e.g. Adams and Laughlin, 1997). Determining the reliability of such powerful stellar chronometers is still underway (Bédard et al., 2024; Salaris et al., 2024; Althaus et al., 2012).

11 Conclusions

This chapter contains a synthetic description of the evolution of low- and intermediate-mass stars. The initial stellar mass is the main parameter that determines how stars evolve with time. It affects the rate of evolution while they are fusing H into He in their hot cores. The larger the initial stellar mass, the larger the luminosity and the shorter the duration of the evolution during the main nuclear burning phases. This property allows a direct determination of the ages of stellar systems. After a long journey on the main sequence, stars quickly move away when their central H has been totally converted into He. Their central density and temperature quickly increase under the effects of self-gravity. In the mean time their surfaces become very large and cool, while their luminosities increase even by orders of magnitude. In low-mass stars with masses between a fraction to about twice the mass of the Sun, the central density becomes so high that electrons become degenerate before the central temperature reaches the threshold to ignite He-burning reactions, that convert He into C and O. A strongly electron degenerate He core forms and slowly grows in mass because of the surrounding H-burning shell. In this phase, stars climb along the Red Giant Branch. Only when the He core reaches about half a solar mass are the central density and temperature high enough to allow He ignition. At this point the star is at the Tip of the RGB, but given the almost explosive nature of nuclear energy ignition within a strongly degenerate material, the core very quickly expands and the star moves on to the Horizontal Branch in the HRD, where it stays for almost the whole central He-burning phase. Intermediate-mass stars, with initial mass larger than about two solar masses, such as those present in young star clusters, are able to ignite He before meeting the conditions for strong central degeneracy. The RGB of such clusters are thus much less populated and much less developed than that of older clusters that contain evolved low mass stars. After central He-burning, low- and intermediate-mass stars have a similar structure and follow a common evolution. They are made of a CO core surrounded by a He-rich shell and by an external H-rich envelope. The CO core contracts because of self-gravity, moving toward the ignition of C-burning reactions. However electron neutrino production by weak interactions becomes high enough to consume the energy released by gravitational contraction. The CO core thus becomes degenerate and grows only because of the material processed by the surrounding He- and H-burning shells, that ignite in a series of periodic thermal pulses that characterize the Asymptotic Giant Branch phase. However, the nuclear growth of the core is challenged by strong stellar winds mainly produced by the formation of dust grains in the cool circum-stellar envelopes of AGB stars. These winds are able to evaporate the whole H-rich envelopes before the CO core reaches the Chandrasekhar mass limit, at which point the star should collapse because not even a strongly electron degenerate core could support its own weight. Instead, a strongly electron degenerate CO core, of mass below M_{Ch} , surrounded by a very thin He- and eventually H-rich envelope is left by low- and intermediate-mass star, at the end of their nuclear evolution. These stars begin a new life whose duration may be even larger than that of their previous life, as compact objects named White Dwarfs.

Low- and intermediate-mass stars are an essential agent in the cycle of the baryonic matter. Their evolution may look less spectacular than that of more massive stars but their number and their persistence are overwhelmingly larger than those of the latter stars, at a level that

²⁹For H-WDs, $X=1$, $\mu_e \sim 1$ and $M_{\text{Ch}} = 5.836M_{\odot}$; however H stars with $M_{\text{ini}} \geq 0.08M_{\odot}$ ignite H before degeneracy set in.

³⁰Their interactions are challenged by unavailability of free momentum states of the outward channel, set by electron degeneracy because all states up to a given energy are already occupied.

almost the whole history of the universe may be recorded and accessed at their surfaces.

A useful database of evolutionary tracks of low- and intermediate-mass stars can be found [here](#).

Acknowledgments

The authors warmly thank their many close collaborators, Paola Marigo, Leo Girardi, Jing Tang, Yang Chen, Xiaoting Fu, Guglielmo Costa, Thanh Nguyen, Francesco Addari, with whom they continuously discussed open questions in this research field. We also thank Dr. Fabian Schneider and Jan Henneco for their careful reading of the original manuscript and many helpful suggestions.

References

- Adams FC and Laughlin G (1997), Apr. A dying universe: the long-term fate and evolution of astrophysical objects. *Reviews of Modern Physics* 69 (2): 337–372. doi:10.1103/RevModPhys.69.337. astro-ph/9701131.
- Addari F, Marigo P, Bressan A, Costa G, Shepherd K and Volpato G (2024), Mar. The Role of the Third Dredge-up and Mass Loss in Shaping the Initial–Final Mass Relation of White Dwarfs. *Astrophys. J.* 964 (1), 51. doi:10.3847/1538-4357/ad2067. 2401.09812.
- Althaus LG, García-Berro E, Isern J, Córscico AH and Miller Bertolami MM (2012), Jan. New phase diagrams for dense carbon-oxygen mixtures and white dwarf evolution. *Astron. Astrophys.* 537, A33. doi:10.1051/0004-6361/201117902. 1110.5665.
- Asplund M, Amarsi AM and Grevesse N (2021), Sep. The chemical make-up of the Sun: A 2020 vision. *Astron. Astrophys.* 653, A141. doi:10.1051/0004-6361/202140445. 2105.01661.
- Bahng J and Schwarzschild M (1961), Sep. Lifetime of Solar Granules. *Astrophys. J.* 134: 312. doi:10.1086/147160.
- Basu S and Antia HM (1997), May. Seismic measurement of the depth of the solar convection zone. *Mon. Not. R. Astron. Soc.* 287: 189–198.
- Bédard A, Blouin S and Cheng S (2024), Mar. Buoyant crystals halt the cooling of white dwarf stars. *Nature* 627 (8003): 286–288. doi:10.1038/s41586-024-07102-y.
- Bergeron P, Ruiz MT and Leggett SK (1997), Jan. The Chemical Evolution of Cool White Dwarfs and the Age of the Local Galactic Disk. *Astrophys. J. Suppl. Ser.* 108 (1): 339–387. doi:10.1086/312955.
- Binney J and Tremaine S (1987). Galactic dynamics.
- Böhm-Vitense E (1958), Jan. Über die Wasserstoffkonvektionszone in Sternen verschiedener Effektivtemperaturen und Leuchtkräfte. Mit 5 Textabbildungen. *Zeitschrift für Astrophysik* 46: 108.
- Bressan AG, Chiosi C and Bertelli G (1981), Sep. Mass loss and overshooting in massive stars. *Astron. Astrophys.* 102 (1): 25–30.
- Bressan A, Chiosi C and Fagotto F (1994), Sep. Spectrophotometric Evolution of Elliptical Galaxies. I. Ultraviolet Excess and Color-Magnitude-Redshift Relations. *Astrophys. J. Suppl. Ser.* 94: 63. doi:10.1086/192073.
- Bressan A, Marigo P, Girardi L, Salasnich B, Dal Cero C, Rubele S and Nanni A (2012), Nov. PARSEC: stellar tracks and isochrones with the PAdova and TRieste Stellar Evolution Code. *Mon. Not. R. Astron. Soc.* 427 (1): 127–145. doi:10.1111/j.1365-2966.2012.21948.x. 1208.4498.
- Buldgen G, Salmon S and Noels A (2019), Jul. Progress in global helioseismology: a new light on the solar modelling problem and its implications for solar-like stars. *Frontiers in Astronomy and Space Sciences* 6, 42. doi:10.3389/fspas.2019.00042. 1906.08213.
- Burrows A and Vartanyan D (2021), Jan. Core-collapse supernova explosion theory. *Nature* 589 (7840): 29–39. doi:10.1038/s41586-020-03059-w. 2009.14157.
- Campos F, Bergeron P, Romero AD, Kepler SO, Ourique G, Costa JES, Bonatto CJ, Winget DE, Montgomery MH, Pacheco TA and Bedin LR (2016), Mar. A comparative analysis of the observed white dwarf cooling sequence from globular clusters. *Mon. Not. R. Astron. Soc.* 456 (4): 3729–3742. doi:10.1093/mnras/stv2911. 1512.03114.
- Cassisi S, Potekhin AY, Salaris M and Pietrinferni A (2021), Oct. Electron conduction opacities at the transition between moderate and strong degeneracy: Uncertainties and impacts on stellar models. *Astron. Astrophys.* 654, A149. doi:10.1051/0004-6361/202141425. 2108.11653.
- Chandrasekhar S (1935), 01. The Highly Collapsed Configurations of a Stellar Mass. (Second Paper.). *Monthly Notices of the Royal Astronomical Society* 95 (3): 207–225. ISSN 0035-8711. doi:10.1093/mnras/95.3.207. <https://academic.oup.com/mnras/article-pdf/95/3/207/18326119/mnras95-0207.pdf>, <https://doi.org/10.1093/mnras/95.3.207>.
- Charbonnel, C. and Zahn, J.-P. (2007). Thermohaline mixing: a physical mechanism governing the photospheric composition of low-mass giants. *Astron. Astrophys.* 467 (1): L15–L18. doi:10.1051/0004-6361:20077274. <https://doi.org/10.1051/0004-6361:20077274>.
- Chen Y, Girardi L, Bressan A, Marigo P, Barbieri M and Kong X (2014), Nov. Improving PARSEC models for very low mass stars. *Mon. Not. R. Astron. Soc.* 444 (3): 2525–2543. doi:10.1093/mnras/stu1605. 1409.0322.
- Chen Y, Girardi L, Fu X, Bressan A, Aringer B, Dal Tio P, Pastorelli G, Marigo P, Costa G and Zhang X (2019), Dec. YBC: a stellar bolometric corrections database with variable extinction coefficients. Application to PARSEC isochrones. *Astron. Astrophys.* 632, A105. doi:10.1051/0004-6361/201936612. 1910.09037.
- Chieffi A, Limongi M and Straniero O (1998), Aug. The Evolution of a 25 M_⊙ Star from the Main Sequence up to the Onset of the Iron Core Collapse. *Astrophys. J.* 502 (2): 737–762. doi:10.1086/305921.
- Clayton DD (1984). Principles of stellar evolution and nucleosynthesis.
- Cummings JD, Kalirai JS, Tremblay PE, Ramirez-Ruiz E and Choi J (2018), Oct. The White Dwarf Initial-Final Mass Relation for Progenitor Stars from 0.85 to 7.5 M_⊙. *Astrophys. J.* 866 (1), 21. doi:10.3847/1538-4357/aadfd6. 1809.01673.
- Cyburtt RH, Amthor AM, Ferguson R, Meisel Z, Smith K, Warren S, Heger A, Hoffman RD, Rauscher T, Sakharuk A, Schatz H, Thielemann FK and Wiescher M (2010), Jul. The JINA REACLIB Database: Its Recent Updates and Impact on Type-I X-ray Bursts. *Astrophys. J. Suppl. Ser.* 189 (1): 240–252. doi:10.1088/0067-0049/189/1/240.
- Cyburtt RH, Fields BD, Olive KA and Yeh TH (2016), Feb. Big bang nucleosynthesis: Present status. *Rev. Mod. Phys.* 88: 015004. doi:10.1103/RevModPhys.88.015004. <https://link.aps.org/doi/10.1103/RevModPhys.88.015004>.
- Demarque P, Guenther DB, Li LH, Mazumdar A and Straka CW (2008), Aug. YREC: the Yale rotating stellar evolution code. Non-rotating version, seismology applications. *Astrophys. Space Sci.* 316 (1-4): 31–41. doi:10.1007/s10509-007-9698-y. 0710.4003.
- Eggenberger P, Meynet G, Maeder A, Hirschi R, Charbonnel C, Talon S and Ekström S (2008), Aug. The Geneva stellar evolution code. *Astrophys. Space Sci.* 316 (1-4): 43–54. doi:10.1007/s10509-007-9511-y.
- Eggleton PP (1971), Jan. The evolution of low mass stars. *Mon. Not. R. Astron. Soc.* 151: 351. doi:10.1093/mnras/151.3.351.

- Eyer L and Mowlavi N (2008), Oct., Variable stars across the observational HR diagram, *Journal of Physics Conference Series*, *Journal of Physics Conference Series*, 118, IOP, pp. 012010, 0712.3797.
- Fowler RH (1926), 12. On Dense Matter. *Monthly Notices of the Royal Astronomical Society* 87 (2): 114–122. ISSN 0035-8711. doi:10.1093/mnras/87.2.114. <https://academic.oup.com/mnras/article-pdf/87/2/114/3623303/mnras87-0114.pdf>, <https://doi.org/10.1093/mnras/87.2.114>.
- Freedman WL and Madore BF (2010), Sep. The Hubble Constant. *Annu. Rev. Astron. Astrophys.* 48: 673–710. doi:10.1146/annurev-astro-082708-101829. 1004.1856.
- Fusi-Pecci F and Renzini A (1975), Mar. On mass loss by stellar wind in population II red giants. *Astron. Astrophys.* 39: 413–419.
- Girardi L (2016), Sep. Red Clump Stars. *Annu. Rev. Astron. Astrophys.* 54: 95–133. doi:10.1146/annurev-astro-081915-023354.
- Goldman SR, van Loon JT, Zijlstra AA, Green JA, Wood PR, Nanni A, Imai H, Whitelock PA, Matsuura M, Groenewegen MAT and Gómez JF (2017), Feb. The wind speeds, dust content, and mass-loss rates of evolved AGB and RSG stars at varying metallicity. *Mon. Not. R. Astron. Soc.* 465 (1): 403–433. doi:10.1093/mnras/stw2708. 1610.05761.
- Gray DF and Kaur T (2019), Sep. A Recipe for Finding Stellar Radii, Temperatures, Surface Gravities, Metallicities, and Masses Using Spectral Lines. *Astrophys. J.* 882 (2), 148. doi:10.3847/1538-4357/ab2f9c.
- Haft M, Raffelt G and Weiss A (1994), Apr. Standard and Nonstandard Plasma Neutrino Emission Revisited. *Astrophys. J.* 425: 222. doi:10.1086/173978. astro-ph/9309014.
- Halm J (1911), Jun. Stars, motion in space, etc. Further considerations relating to the systematic motions of the stars. *Mon. Not. R. Astron. Soc.* 71: 610–639. doi:10.1093/mnras/71.8.610.
- Hayashi C (1961), Jan. Stellar evolution in early phases of gravitational contraction. *Publ. Astron. Soc. Jpn* 13: 450–452.
- Henry LG, Wilets L, Böhm KH, Lelevier R and Levee RD (1959), May. A Method for Automatic Computation of Stellar Evolution. *Astrophys. J.* 129: 628. doi:10.1086/146661.
- Henry LG, Forbes JE and Gould NL (1964), Jan. A New Method of Automatic Computation of Stellar Evolution. *Astrophys. J.* 139: 306. doi:10.1086/147754.
- Herwig F (2005), Sep. Evolution of Asymptotic Giant Branch Stars. *Annu. Rev. Astron. Astrophys.* 43 (1): 435–479. doi:10.1146/annurev.astro.43.072103.150600.
- Hofmeister E, Kippenhahn R and Weigert A (1964), Jan. Sternentwicklung I. Ein Programm zur Lösung der zeitabhängigen Aufbaugleichungen. Mit 3 Textabbildungen. *Zeitschrift für Astrophysik* 59: 215.
- Homan W, Richards A, Decin L, de Koter A and Kervella P (2018), Aug. An unusual face-on spiral in the wind of the M-type AGB star EP Aquarii. *Astron. Astrophys.* 616, A34. doi:10.1051/0004-6361/201832834. 1804.05684.
- Hui-Bon-Hoa A (2021), Feb. Stellar models with self-consistent Rosseland opacities. Consequences for stellar structure and evolution. *Astron. Astrophys.* 646, L6. doi:10.1051/0004-6361/202040095.
- Iben I. J and Renzini A (1983), Jan. Asymptotic giant branch evolution and beyond. *Annu. Rev. Astron. Astrophys.* 21: 271–342. doi:10.1146/annurev.aa.21.090183.001415.
- Iglesias CA and Rogers FJ (1996), Jun. Updated Opal Opacities. *Astrophys. J.* 464: 943. doi:10.1086/177381.
- Itoh N and Kohyama Y (1983), Dec. Neutrino-pair bremsstrahlung in dense stars. I. Liquid metal case. *Astrophys. J.* 275: 858–866. doi:10.1086/161579.
- Kaplan IG (2020). The pauli exclusion principle and the problems of its experimental verification. *Symmetry* 12 (2). ISSN 2073-8994. doi:10.3390/sym12020320. <https://www.mdpi.com/2073-8994/12/2/320>.
- Kippenhahn R, Weigert A and Weiss A (2013). *Stellar Structure and Evolution*. doi:10.1007/978-3-642-30304-3.
- Klessen RS and Glover SC (2023). The first stars: Formation, properties, and impact. *Annual Review of Astronomy and Astrophysics* 61 (Volume 61, 2023): 65–130. ISSN 1545-4282. doi:https://doi.org/10.1146/annurev-astro-071221-053453. <https://www.annualreviews.org/content/journals/10.1146/annurev-astro-071221-053453>, Journal Article.
- Kovetz A, Yaron O and Prialnik D (2009), Jun. A new, efficient stellar evolution code for calculating complete evolutionary tracks. *Mon. Not. R. Astron. Soc.* 395 (4): 1857–1874. doi:10.1111/j.1365-2966.2009.14670.x. 0809.4207.
- Kuiper GP (1938), Nov. The Empirical Mass-Luminosity Relation. *Astrophys. J.* 88: 472. doi:10.1086/143999.
- Kunitomo M, Guillot T, Takeuchi T and Ida S (2017), Mar. Revisiting the pre-main-sequence evolution of stars. I. Importance of accretion efficiency and deuterium abundance. *Astron. Astrophys.* 599, A49. doi:10.1051/0004-6361/201628260. 1702.07901.
- Leavitt HS and Pickering EC (1912), Mar. Periods of 25 Variable Stars in the Small Magellanic Cloud. *Harvard College Observatory Circular* 173: 1–3.
- Low BC (2001), Nov. Coronal mass ejections, magnetic flux ropes, and solar magnetism. *J. Geophys. Res.* 106 (A11): 25141–25164. doi:10.1029/2000JA004015.
- Maeder A (2009). *Physics, Formation and Evolution of Rotating Stars*. doi:10.1007/978-3-540-76949-1.
- Marconi M, Coppola G, Bono G, Braga V, Pietrinferni A, Buonanno R, Castellani M, Musella I, Ripepi V and Stellingwerf RF (2015), Jul. On a New Theoretical Framework for RR Lyrae Stars. I. The Metallicity Dependence. *Astrophys. J.* 808 (1), 50. doi:10.1088/0004-637X/808/1/50. 1505.02531.
- Marigo P, Girardi L, Bressan A, Groenewegen MAT, Silva L and Granato GL (2008), May. Evolution of asymptotic giant branch stars. II. Optical to far-infrared isochrones with improved TP-AGB models. *Astron. Astrophys.* 482 (3): 883–905. doi:10.1051/0004-6361:20078467. 0711.4922.
- Marigo P, Cummings JD, Curtis JL, Kalirai J, Chen Y, Tremblay PE, Ramirez-Ruiz E, Bergeron P, Bladh S, Bressan A, Girardi L, Pastorelli G, Trabucchi M, Cheng S, Aringer B and Tio PD (2020), Jul. Carbon star formation as seen through the non-monotonic initial-final mass relation. *Nature Astronomy* 4: 1102–1110. doi:10.1038/s41550-020-1132-1. 2007.04163.
- Marigo P, Woitke P, Tognelli E, Girardi L, Aringer B and Bressan A (2024), Jan. A&SOPUS 2.0: Low-temperature Opacities with Solid Grains. *Astrophys. J.* 960 (1), 18. doi:10.3847/1538-4357/ad0898. 2310.14588.
- Marino AF, Milone AP, Przybilla N, Bergemann M, Lind K, Asplund M, Cassisi S, Catelan M, Casagrande L, Valcarce AAR, Bedin LR, Cortés C, D'Antona F, Jerjen H, Piotto G, Schlesinger K, Zoccali M and Angeloni R (2013), 11. Helium enhanced stars and multiple populations along the horizontal branch of NGC 2808: direct spectroscopic measurements. *Monthly Notices of the Royal Astronomical Society* 437 (2): 1609–1627. ISSN 0035-8711. doi:10.1093/mnras/stt1993. <https://academic.oup.com/mnras/article-pdf/437/2/1609/13763705/stt1993.pdf>, <https://doi.org/10.1093/mnras/stt1993>.
- McKee CF and Ostriker EC (2007), Sep. Theory of Star Formation. *Annu. Rev. Astron. Astrophys.* 45 (1): 565–687. doi:10.1146/annurev.astro.45.051806.110602. 0707.3514.
- Mihalas D (1970). *Stellar atmospheres*.
- Miller Bertolami, Marcelo Miguel (2016). New models for the evolution of post-asymptotic giant branch stars and central stars of planetary nebulae. *Astron. Astrophys.* 588: A25. doi:10.1051/0004-6361/201526577. <https://doi.org/10.1051/0004-6361/201526577>.
- Milone AP and Marino AF (2022). Multiple populations in star clusters. 2206.10564.

- Morel P and Lebreton Y (2008), Aug. CESAM: a free code for stellar evolution calculations. *Astrophys. Space Sci.* 316 (1-4): 61–73. doi:10.1007/s10509-007-9663-9. 0801.2019.
- Munakata H, Kohyama Y and Itoh N (1985), Sep. Neutrino Energy Loss in Stellar Interiors. *Astrophys. J.* 296: 197. doi:10.1086/163436.
- O'Dell CR, Sabbadin F and Henney WJ (2007), Oct. The Three-Dimensional Ionization Structure and Evolution of NGC 6720, The Ring Nebula. *Astron. J.* 134 (4): 1679–1692. doi:10.1086/521823.
- Palla F and Stahler SW (1993), Nov. The Pre-Main-Sequence Evolution of Intermediate-Mass Stars. *Astrophys. J.* 418: 414. doi:10.1086/173402.
- Pasquini, L., Mauas, P., Käufel, H. U. and Cacciari, C. (2011). Measuring helium abundance difference in giants of ngc 2808. *Astron. Astrophys.* 531: A35. doi:10.1051/0004-6361/201116592. <https://doi.org/10.1051/0004-6361/201116592>.
- Pauli W (1925), Feb. Über den Zusammenhang des Abschlusses der Elektronengruppen im Atom mit der Komplexstruktur der Spektren. *Zeitschrift für Physik* 31 (1): 765–783. doi:10.1007/BF02980631.
- Paxton B, Bildsten L, Dotter A, Herwig F, Lesaffre P and Timmes F (2011), Jan. Modules for Experiments in Stellar Astrophysics (MESA). *Astrophys. J. Suppl. Ser.* 192 (1), 3. doi:10.1088/0067-0049/192/1/3. 1009.1622.
- Prša A, Harmanec P, Torres G, Mamajek E, Asplund M, Capitaine N, Christensen-Dalsgaard J, Depagne É, Haberleiter M, Hekker S, Hilton J, Kopp G, Kostov V, Kurtz DW, Laskar J, Mason BD, Milone EF, Montgomery M, Richards M, Schmutz W, Schou J and Stewart SG (2016), Aug. Nominal Values for Selected Solar and Planetary Quantities: IAU 2015 Resolution B3. *Astron. J.* 152 (2), 41. doi:10.3847/0004-6256/152/2/41. 1605.09788.
- Qiu D, Tian HJ, Wang XD, Nie JL, von Hippel T, Liu GC, Fouesneau M and Rix HW (2021), Apr. Precise Ages of Field Stars from White Dwarf Companions in Gaia DR2. *Astrophys. J. Suppl. Ser.* 253 (2), 58. doi:10.3847/1538-4365/abe468. 2012.04890.
- Raffelt G and Weiss A (1995), Feb. Red giant bound on the axion-electron coupling reexamined. *Phys. Rev. D* 51 (4): 1495–1498. doi:10.1103/PhysRevD.51.1495. hep-ph/9410205.
- Reimers D (1975), Jan. Circumstellar absorption lines and mass loss from red giants. *Memoires of the Societe Royale des Sciences de Liege* 8: 369–382.
- Reimers D (1977), Oct. On the absolute scale of mass-loss in red giants. I. Circumstellar absorption lines in the spectrum of the visual companion of alpha¹Her. *Astron. Astrophys.* 61: 217–224.
- Ripepi V, Molinaro P, Musella I, Marconi M, Leccia S and Eyer L (2019), May. Reclassification of Cepheids in the Gaia Data Release 2. Period-luminosity and period-Wesenheit relations in the Gaia passbands. *Astron. Astrophys.* 625, A14. doi:10.1051/0004-6361/201834506. 1810.10486.
- Rosseland S (1924), May. Note on the absorption of radiation within a star. *Mon. Not. R. Astron. Soc.* 84: 525–528. doi:10.1093/mnras/84.7.525.
- Russell HN (1914), May. Relations Between the Spectra and Other Characteristics of the Stars. *Popular Astronomy* 22: 275–294.
- Salaris M, Cassisi S, Pietrinferni A and Hidalgo S (2022), Feb. The updated BASTI stellar evolution models and isochrones - III. White dwarfs. *Mon. Not. R. Astron. Soc.* 509 (4): 5197–5208. doi:10.1093/mnras/stab3359. 2111.09285.
- Salaris M, Blouin S, Cassisi S and Bedin LR (2024), Mar. Ne22 distillation and the cooling sequence of the old metal-rich open cluster NGC 6791. *arXiv e-prints*, arXiv:2403.02790doi:10.48550/arXiv.2403.02790. 2403.02790.
- Salpeter EE (1954), Sep. Electrons Screening and Thermonuclear Reactions. *Australian Journal of Physics* 7: 373. doi:10.1071/PH540373.
- Saumon D, Blouin S and Tremblay PE (2022), Nov. Current challenges in the physics of white dwarf stars. *Phys. Rep.* 988: 1–63. doi:10.1016/j.physrep.2022.09.001. 2209.02846.
- Schröder KP and Cuntz M (2005), Sep. A New Version of Reimers' Law of Mass Loss Based on a Physical Approach. *Astrophys. J. Lett.* 630 (1): L73–L76. doi:10.1086/491579. astro-ph/0507598.
- Scuflaire R, Théado S, Montalbán J, Miglio A, Bourge PO, Godart M, Thoul A and Noels A (2008), Aug. CLÉS, Code Liégeois d'Évolution Stellaire. *Astrophys. Space Sci.* 316 (1-4): 83–91. doi:10.1007/s10509-007-9650-1. 0712.3471.
- Seaton MJ (2005), Sep. Opacity Project data on CD for mean opacities and radiative accelerations. *Mon. Not. R. Astron. Soc.* 362 (1): L1–L3. doi:10.1111/j.1365-2966.2005.00019.x. astro-ph/0411010.
- Siess L (2007), Dec. Evolution of massive AGB stars. II. model properties at non-solar metallicity and the fate of Super-AGB stars. *Astron. Astrophys.* 476 (2): 893–909. doi:10.1051/0004-6361:20078132.
- Smalley B (2005), Jan. T_{eff} and log g determinations. *Memorie della Societa Astronomica Italiana Supplementi* 8: 130. doi:10.48550/arXiv.astro-ph/0509535. astro-ph/0509535.
- Straniero O, Pallanca C, Dalessandro E, Domínguez I, Ferraro FR, Giannotti M, Mirizzi A and Piersanti L (2020), Dec. The RGB tip of galactic globular clusters and the revision of the axion-electron coupling bound. *Astron. Astrophys.* 644, A166. doi:10.1051/0004-6361/202038775. 2010.03833.
- Tononi J, Torres S, García-Berro E, Camisassa ME, Althaus LG and Rebassa-Mansergas A (2019), Aug. Effects of ²²Ne sedimentation and metallicity on the local 40 pc white dwarf luminosity function. *Astron. Astrophys.* 628, A52. doi:10.1051/0004-6361/201834267. 1906.08009.
- Trampedach R, Stein RF, Christensen-Dalsgaard J, Nordlund and Asplund M (2014), Dec. Improvements to stellar structure models, based on a grid of 3D convection simulations - II. Calibrating the mixing-length formulation. *Mon. Not. R. Astron. Soc.* 445 (4): 4366–4384. doi:10.1093/mnras/stu2084. 1410.1559.
- VandenBerg DA, Edvardsson B, Eriksson K and Gustafsson B (2008), Mar. On the Use of Blanketed Atmospheres as Boundary Conditions for Stellar Evolutionary Models. *Astrophys. J.* 675 (1): 746–763. doi:10.1086/521600. 0708.1188.
- Ventura P, D'Antona F and Mazzitelli I (2008), Aug. The ATON 3.1 stellar evolutionary code. A version for asteroseismology. *Astrophys. Space Sci.* 316 (1-4): 93–98. doi:10.1007/s10509-007-9672-8.
- Vink JS (2022), Aug. Theory and Diagnostics of Hot Star Mass Loss. *Annu. Rev. Astron. Astrophys.* 60: 203–246. doi:10.1146/annurev-astro-052920-094949. 2109.08164.
- Weaver TA, Zimmerman GB and Woosley SE (1978), Nov. Presupernova evolution of massive stars. *Astrophys. J.* 225: 1021–1029. doi:10.1086/156569.
- Weiss A and Schlattl H (2008), Aug. GARSTEC—the Garching Stellar Evolution Code. The direct descendant of the legendary Kippenhahn code. *Astrophys. Space Sci.* 316 (1-4): 99–106. doi:10.1007/s10509-007-9606-5.
- Weiss A, Hillebrandt W, Thomas HC and Ritter H (2004). Cox and Giuli's Principles of Stellar Structure.
- Xu Y, Takahashi K, Goriely S, Arnould M, Ohta M and Utsunomiya H (2013). Nacre ii: an update of the nacre compilation of charged-particle-induced thermonuclear reaction rates for nuclei with mass number $a \leq 16$. *Nuclear Physics A* 918: 61–169. ISSN 0375-9474. doi:<https://doi.org/10.1016/j.nuclphysa.2013.09.007>. <https://www.sciencedirect.com/science/article/pii/S0375947413007409>.